DEUTSCHES ELEKTRONEN-SYNCHROTRON DESY

DESY 72/16
March 1972

On the Movement of Bubbles in a Medium-Sized Bubble Chamber

by

G. Harigel
CERN, Geneva

and

G. Horlitz, S. Wolff
Deutsches Elektronen-Synchrotron DESY, Hamburg

2 HAMBURG 52 · NOTKESTIEG 1

ON THE MOVEMENT OF BUBBLES IN A MEDIUM-SIZED BUBBLE CHAMBER

G. Harigel
CERN, Geneva
and
G. Horlitz, S. Wolff
DESY, Hamburg

ABSTRACT

Bubble movement was measured in the 85 cm hydrogen bubble chamber at DESY as a function of flash delay, liquid temperature, and static pressure. The displacement of bubbles, photographed with a 1 : 1 magnification bright field optic, could be explained by a superposition of three effects: (1) movement of the liquid due to its compressibility, (2) inertia forces and (3) buoyancy forces.

1. INTRODUCTION

With the increased energy of the latest accelerators, with the trend towards the investigation of reactions of high momentum particles, and with the construction of very large bubble chambers with high magnetic fields, the demand for a greater precision in momentum measurement goes hand in hand. This will be achieved partially by measuring longer track segments with higher curvatures (due to the increased volume and higher magnetic field, respectively); partially by more sophisticated optics of the chambers, and finally by more precise automatic track measuring devices for the bubble chamber film. There remain yet to be more fully investigated the important questions concerning the thermodynamic behaviour of liquids in a bubble chamber; that is, the motion of liquid bulk and gas bubbles, as well as microscopic and macroscopic temperature fluctuations.

Previous experiments conducted in the 85 cm bubble chamber at DESY concerned themselves with the density, the growth, and the recompression time of bubbles in liquid hydrogen and deuterium as a function of the expanded pressure, static pressure, and temperature of the liquid, using a one to one optical magnification [1), 2), 3)].

An important by-product of these experiments was the information obtained concerning the movement of bubbles and liquid in a small part of the bubble chamber. In spite of the fact that at present

no sufficient experimental data are available for the derivation of general laws of track distortion and accuracy of momentum determination, we would nevertheless like to discuss here some of the measurements made. For the better understanding of all effects involved in the movement of bubbles and liquid, we will describe their behaviour for the entire time interval between two successive expansions, rather than concentrate only on the small (and important) interval between the injection of the particle beam into the expanded "bath-tub" chamber and the moment of photography. In principle, one can learn from our results how to shift optimally the injection time of particles relative to the pressure minimum and how to optimize other essential parameters such as liquid temperature, expanded pressure, static pressure, for the operation of a bubble chamber.

At the moment, there is no complete theoretical explanation for the results obtained. Nevertheless they can form a basis for further systematic studies, using our optical set-up with the DESY bubble chamber, as well as with other chambers of the bath-tub type.

Measurements obtained with the DUBNA 100 cm hydrogen bubble chamber[4] gave interesting results for the track distortion as a function of flash delays from 1 to 4 ms, as well as indicated liquid motion and random track curvatures. Similar measurements are being currently conducted in the CERN 2 m bubble chamber using the standard optics[5] and some of them have been published recently[6].

2. EXPERIMENTAL ARRANGEMENT

A detailed description of the experimental set-up can be found in [1), 2)]. Only the essential features are repeated here:

The 85 cm bubble chamber at DESY, filled with liquid hydrogen, was exposed to an electron beam (beam profile Δz = 1 cm, Δy = 10 cm) of approx. 2 GeV/c; the pulse length was approx. 10 μs, and its jitter $\pm$ 5 μs. The chamber was operated without a magnetic field.

The thermodynamic conditions for the experiment reported here are summarized in table 1.

For each of the 4 temperatures used the aim was to maintain the same expanded pressure for the same cycle length, but it was impossible to avoid pressure oscillations after completion of the expansion-recompression cycle (cf. fig. 1).

The beam was always injected into the chamber at the pressure minimum.

Schematic drawings of the bubble chamber and the arrangement of optics are given in figs. 2 and 3. The piston (diameter 312 mm) is on the top of the chamber (total volume approx. 220 liters); the 3 ribs are placed between the expansion system and the fiducial volume (approx. 130 liters) in order to homogenize the flow of the liquid and the distribution of the pressure during the expansion cycle.

A one to one magnification bright field optical system was mounted on the downstream camera hole (at beam plane height). A lens with a focal length of 200 mm (Edixar, F = 1 : 4.5), in combination with a focal length doubler (Telemac Vario 2X), was used. In the medium chamber plane the depth of focus was a few millimetres.

In order to obtain high time resolution for the measurement of bubble growth, the flash tubes (Edgerton, Germershausen & Grier; Xenon high pressure tubes, FX 45) were operated at low energies, which gave a light pulse length of approx. 20 μs fwhm. A high sensitivity film was used (ADOX, SCF Supertype A, 24/10 DIN, panchromatic).

Two types of pictures were taken (20 for each condition):

a) Single exposure of tracks with flash delays of
0.3, 0.5, 0.7, 1.0, 1.5, 2.0, 2.5, 3.0,
3.5, 4.0, 4.5, 5.0, 6.0, 7.0, 8.0, 9.0,
10, 15, 20, 25, 30, 35, 40, 50,
60, 70, 80, 90, 100, 120, 140, 160,
180, 200 ms,

b) Double exposure of the same tracks with flash delays of
1 and 6 ms, 6 and 11 ms, 11 and 16 ms, 16 and 21 ms.

A total of ca. 8.000 pictures was taken for the ca. 400 different chamber conditions indicated above.

Double exposure was achieved by two flash tubes. The tubes were separated by a semi-transparent mirror and were placed in such a way that their light was focussed into the camera lens (cf. fig. 3). They were fired one after the other, using a light intensity providing the best contrast for the first and the second track images on the film.

3. RESULTS

Most of the results concerning bubble density, bubble growth and recompression time as functions of various bubble chamber operating conditions have already been published [1), 2)]. In the present paper we will describe phenomena concerning the movement of single bubbles and their behaviour over a long range of time.

The phenomena observed will be discussed in detail for 25 K temperature. Figs. 4a - 15a and 4b - 15b are photographs of single exposures, which are characteristic of the behaviour of the bubbles over a large range of flash delays for the lowest and highest static chamber pressures used (3.9 and 5.4 kp/cm^2 at 25 K respectively). Figs. 16 - 19 are photographs obtained by double exposure of the same tracks at the above temperatures with flash delays up to 21 ms for a static pressure of 3.9 kp/cm^2.

Above a certain magnitude of flash delay all single bubbles show two very distinct characteristics:

a) They develop a "schlieren-tail", which can be interpreted as the path traversed by a bubble relative to the surrounding liquid.
b) Their shape changes from spherical to non-spherical.

However, a bubble string along the path of a particle shows:

a) Severe random deviations of bubbles from the overall trajectory, which becomes more important with increasing flash delay.
b) Interference of neighbouring bubbles such as the effect of bubble coalescence, relative movement, distortion, "explosion" etc.

The measurement of the length and the direction of the schlieren-tail as a function of time gives information about the displacement and the speed of the bubbles relative to the surrounding liquid. The results will be compared with a direct measurement of the displacement of bubbles relative to the coordinate system of the cameras, derived from photos taken with a double exposure.

3.1. Movement of bubbles relative to the surrounding liquid

The displacement of a bubble relative to the surrounding liquid is marked by a "schlieren-tail", which is visible on the photographs (figs. 8a - 15a, 8b - 15b). Schlieren-phenomena in liquids are normally caused by differences between the temperatures of the liquid in the schlieren region and of the undistorted bulk liquid.

In fact, during the period of bubble growth a thin layer of liquid at the surface of a bubble is reduced in temperature due to the withdrawal of heat necessary for the formation of the vapour within the bubble.

On the other hand, for recompression one has to apply an over-pressure to the liquid in order to recondense bubbles as fast as possible. Consequently, during the recompression period not only the heat of evaporation is regained, but an additional amount of irreversible heat is produced. This heat will increase the temperature around the bubble with the effect that the bubble is surrounded by a layer of liquid with a temperature higher than that of the bulk liquid.

If a bubble moves relative to the surrounding liquid, parts of the cold or hot surface-layer are released within the liquid, thus producing the schlieren-phenomena and tracing the path of the bubble within the liquid.

The length of the schlieren-tail as a function of time was measured on the film by means of a microscope (Leitz, magnification 2 x 12.5).

As a hypothesis one can assume that bubble movement relative to the liquid is the result of two forces: of buoyancy forces due to gravity and of inertia forces due to the acceleration of liquid by the expansion system. Buoyancy forces always cause bubbles to move upwards. Inertia forces can change their direction depending on the oscillations of the mechanical system liquid-piston. Indeed, the results of our measurements show in the first phase a bubble movement downwards. Since the expansion system is on the top of the chamber, we start the recompression with a fast piston movement downwards and consequently with an acceleration much larger than gravity of all liquid elements in this direction. Then one can easily show that vapour bubbles with a density smaller than that of the liquid will move downwards. In fact, the direction of bubble movement in the downward phase is identical with the direction of acceleration. Extrapolation of the inclined schlieren-tails backwards (through the gaps between the rips of fig. 2) will end in the piston region. This indicates that the spherical wave produced by the piston must be responsible for this part of bubble motion. After the expansion system has come to rest, the movement of a bubble is entirely governed by buoyancy forces. In the period between these extreme cases a superposition of the two forces results in bubble paths as shown in figs. 14b and 15b. The tail can show several zig-zags, which can be closely related to pressure oscillations in the bubble chamber.

Fig. 20 illustrates schematically the behaviour of a bubble during the time between creation and complete recompression. The bubble (full circles) is created in position 0 at the time t_o. In position 1 the bubble has grown during the time interval Δt_1, but a measurable displacement relative to the liquid can not yet be detected (i.e. there exists no detectable schlieren-tail). In position 2 the bubble has been displaced towards the bottom by an amount L_1 during a time interval Δt_2. Now buoyancy forces become important causing the bubble to move upwards until position 3 is reached. Here, due to a reversal of piston acceleration, the direction of bubble movement reverses (position 4). Finally, in position 5, the piston is at rest and the bubble ascends due to buoyancy forces alone. The amount of displacement L_2 is measured during the time interval Δt_4.

The results of the measurements depicted in figs. 21, 22 and 23 can now be subdivided in the following way:

3.1.1. Movement of the bubble downwards

The measured lengths of the schlieren-tail as functions of flash delays can be represented by two straight lines (tolerances given for the measured points indicate maximum and minimum values). The line with a larger slope represents the real displacement of the bubble, whereas the line beginning later must be interpreted as an extension of the hot liquid tail. The prolongation of the latter is independent of the static chamber pressure. The extension of the hot liquid tail was already present before the bubble changed its direction, but this effect is small and will be ignored in our evaluation.

The time at which the inertia movement of the bubble starts downwards (relative to the bulk of the liquid), depends on the liquid temperature and on the bubble radius. This displacement commences earlier at high temperatures when smaller bubbles are present, whereas it starts later at low temperatures which give rise to larger bubbles (fig. 24). The total time between the creation of a bubble and the start of its upward movement (figs. 25 and 26), show characteristic features: the time intervals are short for small bubbles at high temperatures and long for large bubbles at low temperatures.

In figs. 27 and 28 amounts and speeds of the initial downward movements of the bubbles due to inertia forces are displayed as functions of the dynamic pressure amplitude $\Delta P = P_{min} - P_s$. They can be fitted by straight lines passing through the origin. The values for their inclinations are listed in table 2. They increase with decreasing temperatures and increasing bubble radii. From tab. 1 can be seen that the cycle length of the expansion-system was kept constant through the whole experiment. If we consider the expansion-system as a harmonic oscillator with frequency f, $\omega = 2\pi f$, the acceleration of the masses of piston and liquid must be proportional $\omega^2 \times h$ (h = maximum piston displacement). As far as parasitic boiling can be neglected, the dynamic pressure amplitude in a bubble chamber is proportional to the mechanical amplitude of the expansion-system. Consequently, at constant cycle length

(ω = constant) all inertia effects must be proportional to ΔP. The linear dependence between ΔP and both bubble displacement and bubble speed in the downward direction indicates that the assumption of inertia forces to be responsible for the downward movement seems to be reasonable.

It is difficult to calculate quantitatively the movement of the bubble downwards for a number of reasons: for example, during the recompression process the gas bubble becomes aspherical and changes its volume. The characteristics of the gas as well as the thermodynamic values of the boundary change, simultaneously with a change in the thickness of this layer. The temperature of the gas T *) inside the bubble, the vapour density ρ_V, the liquid density ρ_L, and the dynamic viscosity η change. Numerical values for these quantities for the conditions of the present experiment are given in table 3.

3.1.2. Movement of the bubble upwards

After the piston and the liquid have come to a rest, the lift velocity of bubbles can be measured with good precision up to flash delays of ca. 60 ms. Pictures taken with larger delays show heavy turbulences in the liquid which destroy the physical characteristics of the schlieren-tail. The results are depicted in figs. 29 - 32. As theoretically predicted, lift velocity depends only slightly on temperature and static pressure in the normal operating range of the chamber, but depends considerably on the bubble radius. A change in the speed of displacement occurs when a radius of R $\sim$0.1 mm is reached during the recompression process. Down to this bubble radius the measured displacements can be fitted by a straight line; i.e. the bubble lift velocity is governed by turbulent flow and is therefore constant in time. Numerical values are summarized in table 4, together with theoretical predictions for the corresponding large bubbles in hydrogen ($R_{theor} > 0.2$ mm)[7), 3)] according to formula

$$v = \sqrt[5]{\frac{4 \cdot \rho_V \cdot \sigma^2}{12 \cdot \pi \cdot \rho_L^2 \cdot \eta}}$$

As is easily seen, both are in reasonable agreement.

*) T (P_{min}) and T (P_s) are the equilibrium temperatures corresponding to the instantaneous pressures in the bubbles at P = P_{min} and P = P_s resp.

For bubble radii $R < 0.1$ mm, a significant decrease in lift velocity is found (cf. figs. 31 and 32). The expected proportionality $v \sim R^2$ for laminar flow is not quantitatively checked due to the limited data available from the present experiment.

3.2. Displacement of the bubble together with the surrounding liquid

A bubble moves not only relative to, but also partially together with, the surrounding liquid. This displacement of the bubble is caused by the movement of the liquid bulk during the expansion-recompression cycle, and depends on the compressibility of the liquid. The direction of the movement of the bubbles is related to the injection time of the particles; if the bubbles are created before the pressure minimum, they move first upwards and then downwards; but if they are produced after the pressure minimum, then they move only downwards with the liquid. In both cases, the movement ceases when the piston comes to a rest.

The above displacement is a function of the distance from the bubble to the piston, as well as a function of the specific geometry of a bubble chamber and of the piston stroke (volume change).

Oscilloscope pictures of the piston displacement are unavailable for the present experiment. The dependence of volume change on pressure has already been investigated for the DESY bubble chamber[8]. Therefore, idealized curves of the volume change could be derived from the known pressure curves and are sufficient for the present purpose.

The amount of the displacement vs. time is easier to estimate if one makes the following assumptions:

a) The visible (fiducial) volume has a simple rectangular shape.

b) Reflections of pressure waves upon the chamber walls are assumed to be small and can therefore be ignored.

c) The compression of the liquid is assumed to be a linear funtion of the change in volume in the liquid phase.

d) Effects arising from finite sound velocity differ by less than 1 ms throughout the fiducial volume and can therefore be ignored.

With these assumptions the bulk movement of the liquid in the beam plane shows the time dependence indicated in figs. 21, 22, and 23.

3.3. Direct measurement of the total displacement of bubbles

A series of pictures was taken for the four following temperatures with one corresponding static pressure (T = 25 K, 26 K, 27 K, 28 K, P_s = 3.90; 4.70; 5.49; 6.50 kp/cm^2, respectively), by photographing the same bubble tracks twice on one film. The two flash delays differed always by 5 ms.

Pictures with a double exposure permit direct measurement of the direction of the movement of bubbles; one can determine their velocity by measuring the distance between the two corresponding images. Bubble images from the two separate exposures can be recognized, because the size and the shape of the bubble as well as the length of the schlieren-tail at different flash delays has been established from the series of pictures taken with a single exposure.

Fig. 21 shows the result of the present direct measurement at T = 25 K together with the results given in chapters 3.1 and 3.2. The total displacement of the bubble is now to be viewed as the sum of (1) the displacement of the liquid bulk due to its compressibility, (2) the displacement of the bubble relative to the liquid due to inertia forces, and finally of (3) the movement due to buoyancy forces. The results of the direct measurements and the sum of the three components substantiate each other.

At 25 K the maximum displacement of a bubble from its point of creation amounts to 4, 5, and 6 mm which corresponds to the total pressure rise of 2.5, 3.1, and 3.9 kp/cm^2, respectively, at approx. 20 ms after the passage of the particle; after approx. 40, 45, and 50 ms, respectively, the bubble passes through the horizontal level drawn through its point of creation.

Results for T = 25, 26, 27, and 28 K and for the lowest static pressures used in the present experiment are given in fig. 33. The amount of maximum bubble displacement at large flash delays decreases with increasing temperature, but for shorter delays the bubble displacement shows essentially the opposite dependence on temperature. The choice of the optimum operating conditions for a chamber

should not only be based, however, on the above behaviour, but also on the overall appearance of the tracks.

3.4. Overall appearance of track segments

In the previous chapters, a quantitative study of the movement of single, isolated bubbles was made. Now some common features of bubbles which are close to each other will be described. Interference can be seen for bubbles belonging to the same or to neighbouring particle tracks next to vertices or inelastic scatters.

3.4.1. Coalescence of neighbouring bubbles

The decrease with time of the number of bubbles along the track was already investigated in propane[9]. It was shown that this effect is very pronounced for initially high bubble densities, at high temperatures, and for short flash delays. The same behaviour is observed in hydrogen and deuterium. During the process of coalescence, which is responsible for the decrease in bubble density, bubbles are deformed and, thus, can differ remarkably in size. Neighbouring bubbles mutually influence their spatial position, and important random deviations for some bubbles from the original path of the particle can be observed.

3.4.2. Temperature field around bubbles

Bubble tracks which are close to each other influence the relative position of one another. When hot liquid from a bubble or a track segment reaches another bubble or track segment, it can displace and/or deform the latter or even make it "explode". This explosion, which gives the bubbles a fuzzy appearance, may be due to resonance oscillations on the bubble's surface (figs. 11a and 11b).

The degree of displacement of bubbles and track segments is a function of their distance and their age. Quantitative statements, however, require the use of stereo optics to determine precisely the relative position of the bubbles and bubble groups interfering with each other.

3.4.3. Pressure oscillations in the liquid

Pressure oscillations in the liquid caused by vibrations of the piston and multiple reflections of waves on the chamber walls, affect in a random manner the position of track bubbles. They can even reverse the direction of movement of the bubbles during the period of their ascent (cf. figs. 13b and 14b).

3.4.4. Turbulence effects in the liquid

It is beyond the scope of the present paper to give quantitative results for track distortions caused by local turbulent effects. It should be mentioned, however, that the dynamic viscosity decreases rapidly with increasing temperature (cf. table 3). As a result of this and other relevant properties of the liquid and gas, distortions for given flash delays increase remarkably with liquid temperature and static pressure. Random track curvatures in the present experiment are best illustrated in figs. 4a - 6a, 4b - 6b, and 34a - 42a, 34b - 42b, where "a" gives always the lowest and "b" the highest static pressure. A comparison of tracks having identical bubble diameters requires longer flash delays for higher temperatures. Such a comparison demonstrates even better the important increase of distortion with increasing temperatures.

4. CONCLUSIONS AND FUTURE EXPERIMENTS

The dependence of the bubble movement on time was studied in a small segment of the fiducial volume of a classical bath-tub bubble chamber. Particles were always injected during the minimum of the dynamic pressure curve. Using two different methods, the displacement, the speed, and the direction of the movement of the bubbles were determined; good quantitative agreement between the results was found. The correlation between the piston movement on the one hand and the bulk movement of the liquid and the acceleration of bubbles downwards on the other, was investigated. The moment when bubbles due to buoyancy forces began to rise was determined. Bulk movement, acceleration by piston, and buoyancy explain quantitatively actual bubble movement.

The measurements of bubble movement should be repeated under the same thermodynamic conditions for other regions of the chamber. The results now attained allow us then to estimate much better the influence of the movement of individual bubbles on track curvature. A step further would be to extend the experiment to include new injection times for the temperatures already used. For bubble chambers with piston on the top, the degree of bubble displacement can probably be reduced, if the beam is injected before the dynamic pressure minimum is reached.

The results reported here are typical for the DESY bubble chamber, its shape, and its piston speed. The bubble movement will be similar for the CERN 2m and the BNL 80-inch chambers; the amount of the expected displacement, however, will strongly depend on the diameter, the stroke, and the velocity of the piston.

Recently, results of some distortion measurements of 16 GeV/c pion tracks in the CERN 2 m bubble chamber, filled with deuterium, came to our knowledge [6]. These measurements were obtained under a limited range of operating conditions. Systematic deviations from the expected ideal particle path were observed and were found to be symmetric to

the chamber center, both with and without a magnetic field. The observations in the 2 m chamber are in principle not very different from those of the DESY experiment: a look at the geometry of the CERN chamber shows immediately that the heat exchangers and the rib located between the piston and the fiducial volume force the liquid and consequently the bubbles, to move in preferential directions. Here the largest deviations of bubbles from the original path can be found. It would be worthwhile to make complementary measurements in the CERN chamber with special emphasis placed on other injection times of particles and other flash delays, and to map the distortions as a function of these essential parameters.

5. ACKNOWLEDGEMENTS

We are greatly indebted to Professors M.W. Teucher and E. Lohrmann for their continued interest and encouragement in the course of these investigations.

We also thank our bubble chamber team, especially W. Eschricht, H.J. Fiebig, U. Knopf, K.D. Nowakowski, O. Peters and W. Stahlschmidt.

Furthermore, we have to thank the DESY machine group as well as the beam operating crew for the excellent performance of the synchrotron and the beam.

6. REFERENCES

1.	S. Wolff	Blasenbildung und Blasenwachstum in einer mit Wasserstoff und Deuterium gefüllten Blasenkammer, Thesis, Hamburg, (1969), DESY B 1 - 1, (unpublished).
2.	G. Harigel, G. Horlitz S. Wolff	Measurement on the Formation, Growth, and Recompression of Bubbles in Liquid Hydrogen, DESY 67/14 (1967), and Int. Coll. Bubble Chamber Technology, Heidelberg, (1967).
3.	G. Harigel, J. Riche, G. Horlitz, S. Wolff	Numerical Calculations of the Recompression Time of Bubbles in Liquid Hydrogen Bubble Chambers, Geneva, (1968), (unpublished).
4.	V.V. Glogolev E.I. D'Yachkov, E.V. Kozubskij, R.M. Lebedev, Ngo Kuang Zuj, J.S. Saitov	Dynamic Distortion of Particle Tracks in the JINR 100 cm Hydrogen Bubble Chamber, Dubna, Preprint 1-4847, (1969).
5.	L. Voyvodic	Private Communication.
6.	G. Ekspong	Multiple Scattering Residuals on Tracks CERN/D.Ph.II/PHYS. 71-40, July (1971), (unpublished).
7.	V.G. Levich	Physicochemical Hydrodynamics, Gostekhizat, (1959).
8.	G. Horlitz, S. Wolff, G. Harigel	On the Thermodynamics of Bubble Chamber Expansions, DESY 68/43 (1968).

9. G. Harigel, P. Kunkel
M. Scheer

Zur Blasendichte in einer Propan-Blasenkammer,
München, MPI-PA-6/63, (1963),
(unpublished).

7. FIGURE CAPTIONS

1. Pressure-time curves for the present experiment (cf. table 1).

2. Schematic drawing of the vertical section of the 85 cm bubble chamber at DESY. The approximate direction of the bubble movement is indicated. All dimensions are in millimeters.

3. Schematic drawing of the horizontal section of the 85 cm bubble chamber at DESY. Arrangement of the optics for bright field photography.

4-15. Photographs of tracks, taken with 1:1 magnification bright field optics; single exposures blown up to twice their actual size.

4a-15a P_v = 3.34 kp/cm^2, P_s = 3.90 kp/cm^2, T = 25 K

4b-15b P_v = 3.34 kp/cm^2, P_s = 5.40 kp/cm^2, T = 25 K

16-19. Photographs of tracks, taken with 1:1 magnification bright field optics. Double exposure of film with differences in flash delays of 5 ms. P_v = 3.34 kp/cm^2, P_s = 3.90 kp/cm^2, T = 25 K

20. Displacement of a bubble relative to the liquid (schematic). Length L_1 indicates the movement of the bubble downwards, due to inertia forces, the hatched part of the tail -- the superposition of buoyancy and inertia forces, and the dotted part -- the lift due to buoyancy forces alone.

21. Results of measurements for a time interval of 80 ms from the beginning of the expansion cycle at T = 25 K, P_v = 3.34 kp/cm^2 and P_s = 3.90 kp/cm^2.

21/1. (1a) Dynamic pressure.

(1b) Volume change during expansion-recompression.

(2a) Displacement of the liquid bulk in the beam plane due to compression. Zero point for liquid motion is arbitrarily chosen to coincide with the pressure minimum and the injection time of the beam.

(2b) Length L_1 is the schlieren-tail, emerging from the bubble and directed upwards. The measured length's L_1 are connected by two straight lines.

(2c) Length L_2 is the schlieren-tail, directed downwards and measured up to the last point of change in direction. Experimental values are connected by one straight line.

21/2. (3) Bubble radii. Approx. 20 ms after the creation of bubbles, their shape becomes aspherical.

(4a) Speed of liquid displacement due to compression.

(4b/c) Speed of the displacement of bubbles relative to the surrounding liquid, determined by measuring the length of the schlieren-tail, downwards (a) and upwards (b).

(4d) Total speed of bubbles (sum of 4a and 4b resp. 4c).

(4e) Speed of the displacement of bubbles, directly measured from photographs with double exposure of tracks.

21/3. (5a) Displacement of the liquid in beam plane.

(5b) Displacement of bubbles downwards, determined from the length of the schlieren-tails.

(5c) Displacement of the bubbles due to buoyancy forces, determined from the length of the schlieren-tails.

(5d) Total displacement (sum of 5a and 5b resp. 5c).

(5e) Total displacement of bubbles, directly determined from photographs with double exposure of tracks.

22/1/2/3. Results of measurements for a time interval of 80 ms from the beginning of the expansion cycle at T = 25 K, P_v = 3.34 kp/cm^2 and P_s = 4.6 kp/cm^2, cf. captions of figs. 21. As photographs with double exposure were unavailable curves (4e) and (5e) are not given.

23/1/2/3. Results of measurements for a time interval of 80 ms from the beginning of the expansion cycle at T = 25 K, P_v = 3.34 kp/cm^2 and P_s = 5.40 kp/cm^2, cf. captions of figs. 22 and 23. As photographs with double exposure were unavailable curves (4e) and (5e) are not given.

24. The time between bubble creation and start of its inertia movement downwards, as a function of the bubble radius found at the beginning of this movement. Results are given for T = 25, 26, 27, and 28 K and at different static pressures.

25. Time between bubble creation and the end of its movement downwards as a function of the bubble radius at the beginning of this movement. Results are given for T = 25, 26, 27, and 28 K and different static pressures.

26. Duration of bubble movement downwards due to inertia forces as function of the bubble radius at the beginning of this movement. Results are given for T = 25, 26, 27, and 28 K and different static pressures.

27. Speed of bubbles moving downwards relative to the liquid as a function of the difference between minimum and static pressure. Results are given for T = 25, 26, 27, and 28 K and different static pressures.

28. Displacement of bubbles moving downwards relative to the liquid as a function of the difference between minimum and static pressure. The bubble radii at the commencement of this movement are indicated. Results are given for T = 25, 26, 27, and 28 K.

29. Bubble ascent due to buoyancy forces as a function of time at T = 25 K. Results are given for 3 static pressures. It is indicated at which time during the recompression process the bubble decreases to R$\sim$0.1 mm.

30. Bubble ascent due to buoyancy forces as a function of time at T = 26 K. Results are given for 3 static pressures. It is indicated at which time during the recompression process the bubble decreases to R$\sim$0.1 mm.

31. Bubble ascent due to buoyancy forces as a function of time at T = 27 K. Results are given for 3 static pressures. It is indicated at which time during recompression process the bubble decreases to R$\sim$0.1 mm.

32. Bubble ascent due to buoyancy forces as a function of time at T = 28 K. Results are given for 2 static pressures. It is indicated at which time during the recompression process the bubble decreases to R$\sim$0.08 mm.

33. Total displacement of bubbles from their point of creation as a function of time for T = 25, 26, 27, and 28 K and the lowest static pressure. Results are derived from direct measurements with double exposure of the same track. Broken lines give the part of displacement due to inertia forces.

34-42. Photographs of tracks taken with 1:1 magnification bright field optics; single exposures blown up to twice their actual size.

34a, 35a, 36a. P_v = 4.10 kp/cm^2, P_s = 4.70 kp/cm^2, T = 26 K
34b, 35b, 36b. P_v = 4.10 kp/cm^2, P_s = 6.10 kp/cm^2, T = 26 K

36a, 37a, 38a. P_v = 5.00 kp/cm^2, P_s = 5.49 kp/cm^2, T = 27 K
36b, 37b, 38b. P_v = 5.00 kp/cm^2, P_s = 6.98 kp/cm^2, T = 27 K

40a, 41a, 42a. P_v = 6.00 kp/cm^2, P_s = 6.50 kp/cm^2, T = 28 K
40b, 41b, 42b. P_v = 6.00 kp/cm^2, P_s = 7.00 kp/cm^2, T = 28 K

These photographs taken with 1, 3, and 5 ms flash delay should be compared also with figs. 4a, 5a, 6a, and 4b, 5b, 6b at T = 25 K.

Nr.	Temperature T K	Vapour-pressure P_v kp/cm^2	Static Pressure P_s kp/cm^2	Expanded Pressure P_{min_2} kp/cm^2	Piston Stroke h mm	Cycle Length C ms	Bubble Density b b/cm
1	25	3.34 ± 0.06	3.90 ± 0.05	1.25 ± 0.1	17.5 ± 1.0	39.0 ± 1	8 ± 1
2	25	3.34 ± 0.06	4.60 ± 0.05	1.25 ± 0.1	23.0 ± 1.5	37.0 ± 1	8 ± 1
3	25	3.34 ± 0.06	5.40 ± 0.05	1.35 ± 0.1	28.0 ± 3.0	40.0 ± 1	8 ± 1
4	26	4.10 ± 0.10	4.70 ± 0.05	1.80 ± 0.1		38.0 ± 1	22 ± 2
5	26	4.10 ± 0.10	5.40 ± 0.05	1.80 ± 0.1		38.5 ± 1	22 ± 2
6	26	4.10 ± 0.10	6.10 ± 0.05	1.70 ± 0.1		38.5 ± 1	22 ± 2
7	27	5.00 ± 0.04	5.49 ± 0.05	2.85 ± 0.1		34.0 ± 1	32 ± 3
8	27	5.00 ± 0.04	6.00 ± 0.05	2.80 ± 0.1		36.5 ± 1	32 ± 3
9	27	5.00 ± 0.03	6.98 ± 0.05	2.70 ± 0.1		35.5 ± 1	32 ± 3
10	28	6.00 ± 0.05	6.50 ± 0.05	3.70 ± 0.1		36.0 ± 1	45 ± 4
11	28	6.00 ± 0.06	7.00 ± 0.05	3.60 ± 0.1		36.0 ± 1	45 ± 4

TABLE 1

Liquid temperature	Bubble radius at the beginning of inertia movement	Bubble displacement downwards / pressure rise
T_L	R	$s/(\Delta P)$
K	cm	$cm/(kp/cm^2)$
25	0.044	0.082
26	0.021	0.029
27	0.011	0.019
28	0.010	0.012

TABLE 2

Liquid temperature	T_L	25	26	27	28	K
	P_v	3.3	4.1	5.0	6.0	kp/cm^2
Expanded pressure	P_{min}	1.3	1.8	2.8	3.6	kp/cm^2
Static pressure	P_s	3.9	4.7	7.0	7.0	kp/cm^2
Maximum bubble radius	R	0.045	0.021	0.011	0.010	cm
Temperature inside the bubble at expanded pressure	$T(P_{min})$	21.0	22.5	24.2	25.5	K
Temperature inside the bubble at static pressure	$T(P_s)$	25.8	26.7	28.9	28.9	K
Density of the liquid	$\rho_L(T_L)$	6.45	6.28	6.10	5.90	10^{-2} g/cm^3
Density of the vapour at expanded pressure	$\rho_V(P_{min})$	8.03	11.5	17.0	22.1	10^{-4} g/cm^3
Density of the vapour at static pressure	$\rho_V(P_s)$	23.6	28.2	43.2	43.2	10^{-4} g/cm^3
Surface tension at expanded pressure	$\sigma(P_{min})$	1.81	1.57	1.30	1.10	g/s^2
Surface tension at static pressure	$\sigma(P_s)$	1.06	0.76	0.58	0.58	g/s^2
Dynamic viscosity at expanded pressure	$\eta(P_{min})$	1.25	1.12	0.98	0.90	g/s·cm
Lynamic viscosity at static pressure	$\eta(P_s)$	0.88	0.84	0.74	0.74	g/s·cm
Isentropic compressibility of the liquid	β	592	522	457	392	kp/cm^2
Reynold number/speed	$\frac{\rho_L(T_L)\cdot R}{\eta(P_s)}$	3.3	1.6	0.9	0.8	10^{-3} s/cm

TABLE 3

Temperature	Static pressure	Lift velocity for	
		$R > 0.2$ mm	$R > 0.10 \pm 0.03$ mm
T_L	P_s	Theory	Experiment
K	kp/cm^2	cm/s	cm/s
25	3.9	14.8	17.0 ± 0.5
25	4.6	14.8	15.5 ± 2.5
25	5.4	14.5	17.0 ± 1.0
26	4.7	14.9	18.0 ± 2.0
26	5.4	14.6	17.5 ± 1.5
26	6.1	14.3	20.0 ± 2.5
27	5.5	14.8	12.5 ± 1.0
27	6.0	14.6	19.0 ± 2.0
27	7.0	14.0	18.0 ± 1.5
28	6.5	14.5	13.0 ± 1.0
28	7.0	14.2	15.5 ± 0.5

TABLE 4

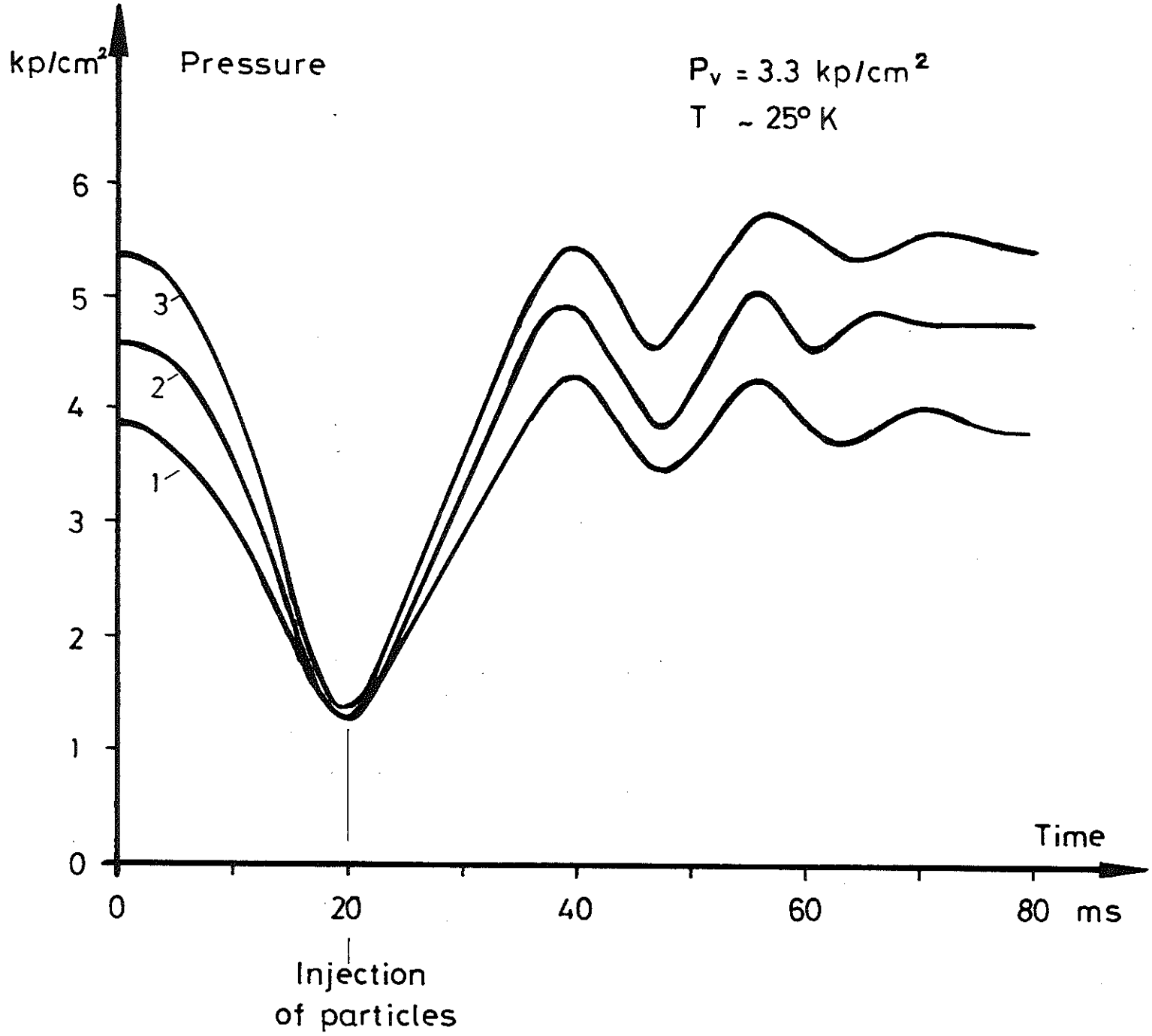
kp/cm²
Pressure
P_v = 3.3 kp/cm²
T ~ 25° K
6
5
4
3
2
1
0
3
2
1
Time
0
20
40
60
80 ms
Injection
of particles

FIG. 1

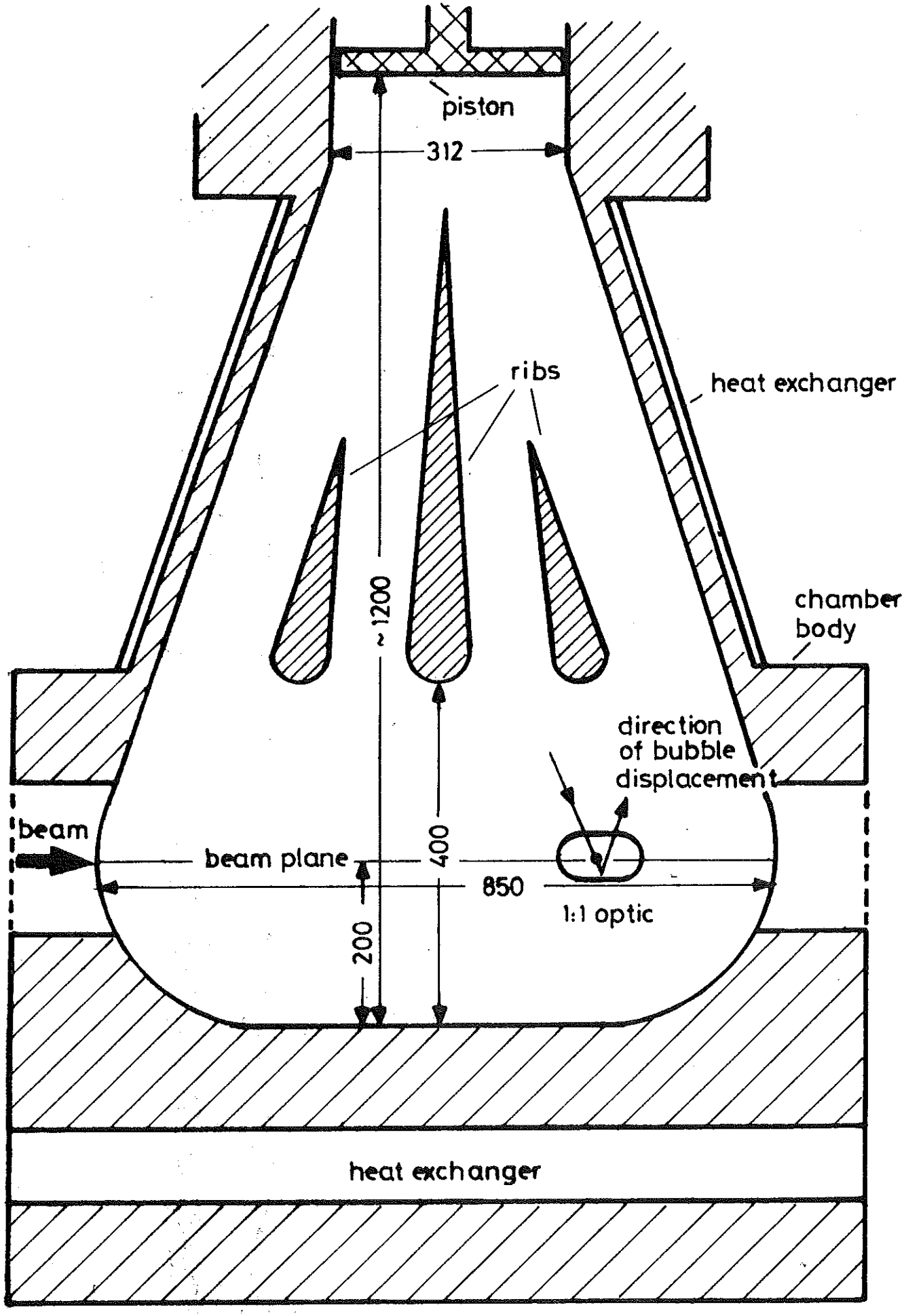

85 cm BUBBLE CHAMBER AT DESY (schematic)

FIG. 2

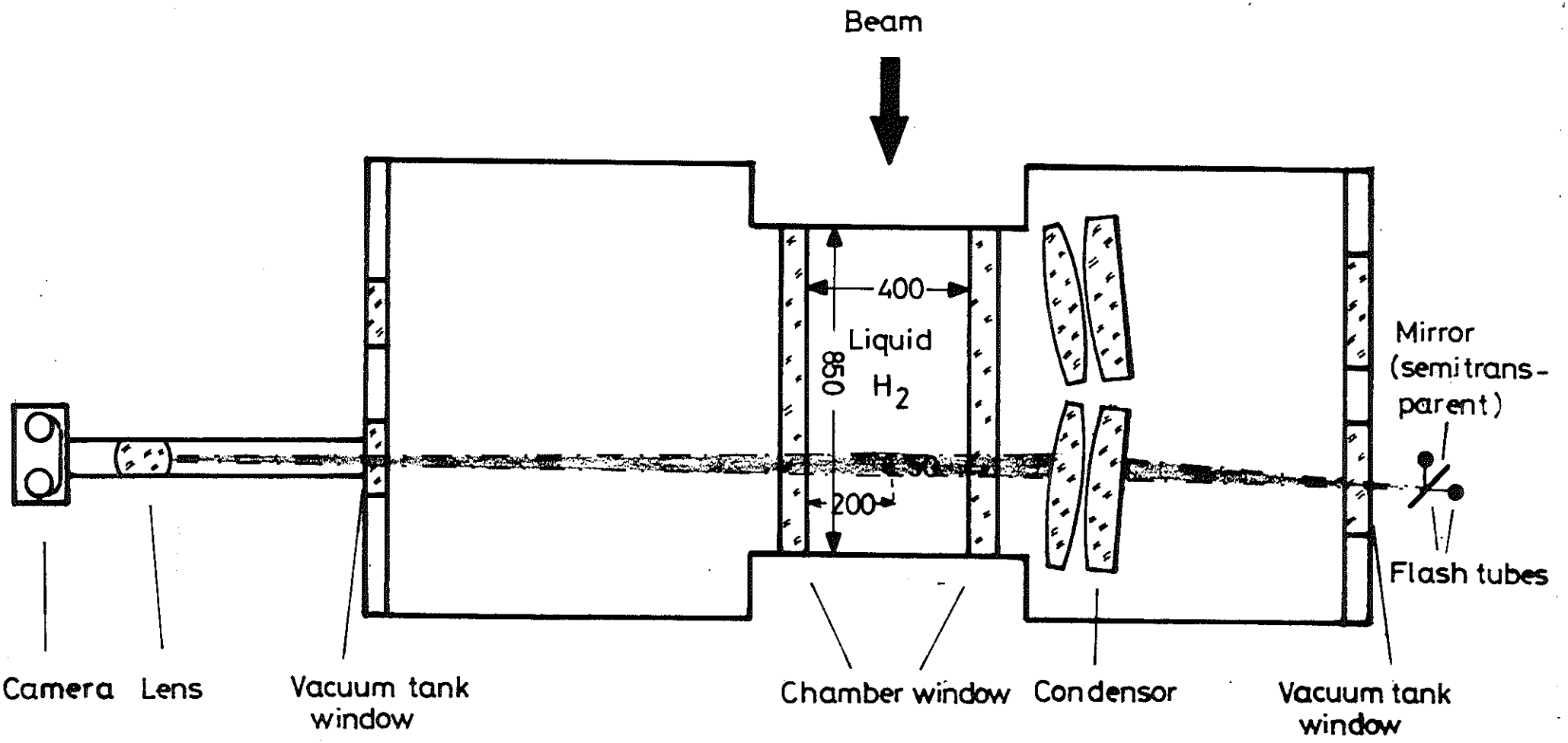

ARRANGEMENT OF OPTICS

(horizontal view, not exactly in scale)

FIG. 3

Figs. 4a - 15a $T = 25$ K

$P_v = 3.34$ kp/cm^2

$P_s = 3.90$ kp/cm^2

$P_{min} = 1.25$ kp/cm^2

Fig. 4a Δt = 1 ms, R ∿0.20 mm, b ∼ 9 bubbles/cm

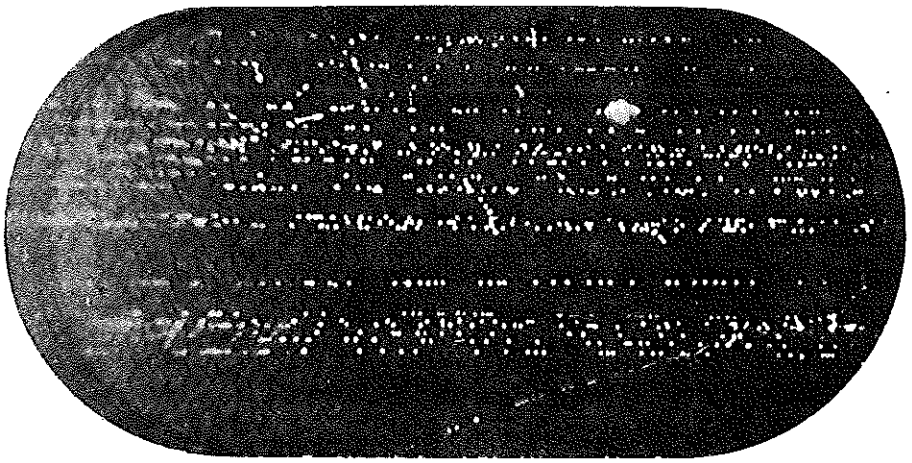

Top(piston) of the chamber

Spherical bubbles

Bottom of the chamber

Fig. 5a Δt= 3 ms, R∼0.35 mm, b∼9 bubbles/cm

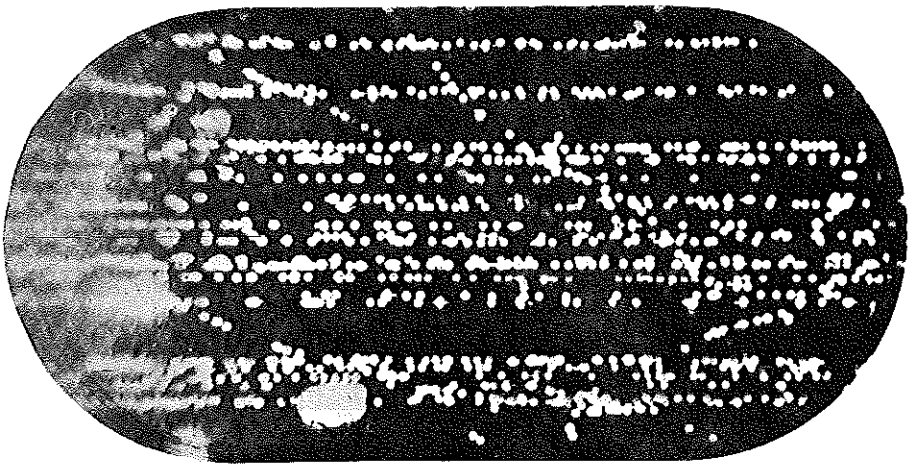

Fig. 6a Δt = 5 ms, R∿0.45 mm, b∿8 bubbles/cm

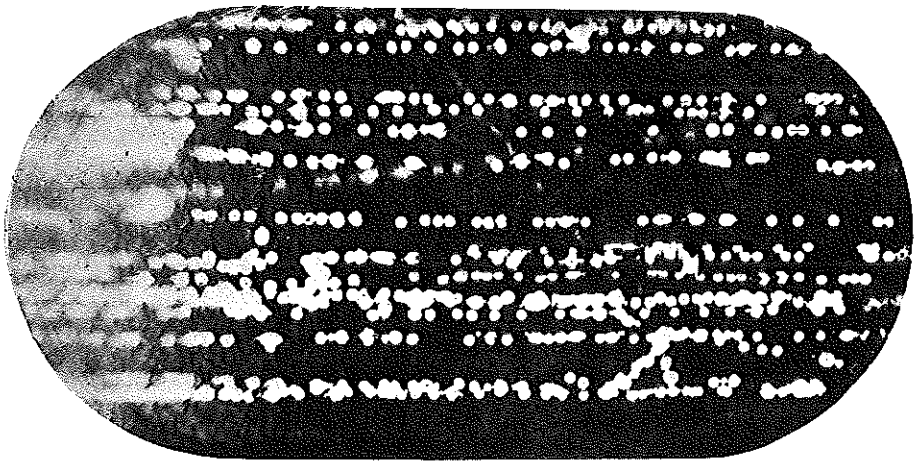

0 1 2 3 4 5 6 cm

Fig. 7a $\Delta t = 7$ ms, $R \sim 0.52$ mm, $b \sim 7$ bubbles/cm

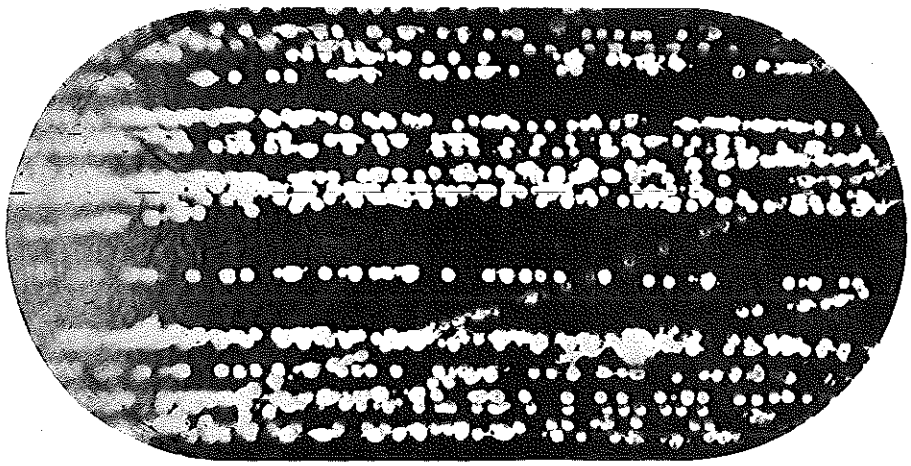

Determination of the center of the bubbles becomes difficult

Fig. 8a $\Delta t = 9$ ms, $R \sim 0.47$ mm, $b \sim 7$ bubbles/cm

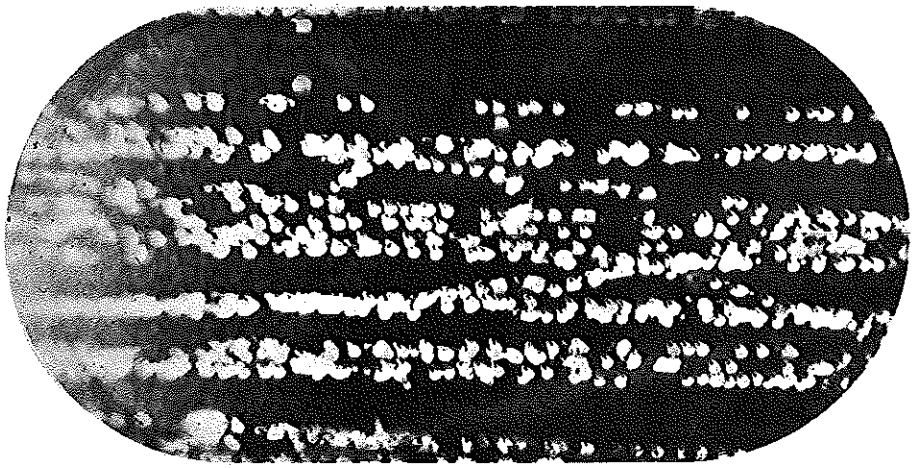

Beginning of the schlieren-tail development. Good visible track distortion

Fig. 9a $\Delta t = 10$ ms, $R \sim 0.42$ mm, $b \sim 7$ bubbles/cm

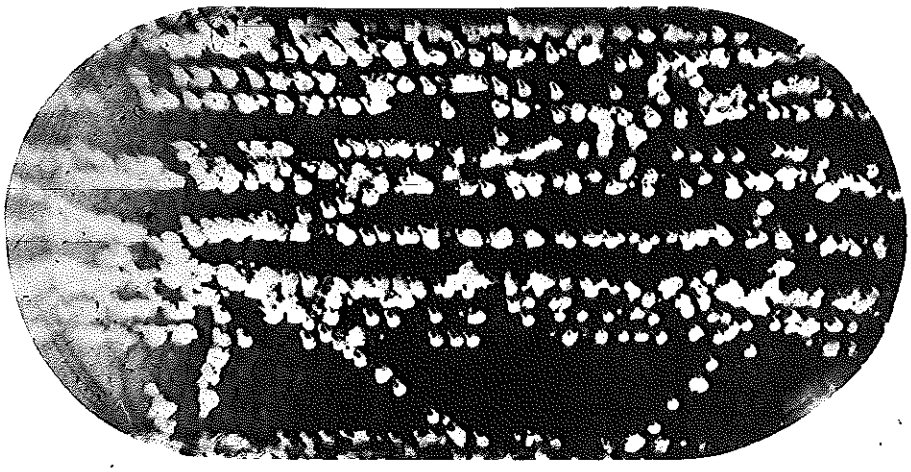

Fig. 10a $\Delta t = 15$ ms, $R \sim 0.38$ mm

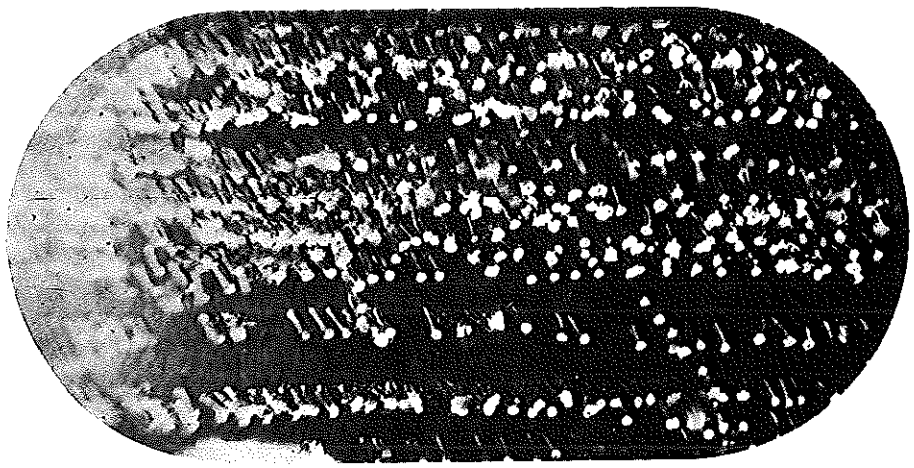

Fig. 11a $\Delta t = 20$ ms, $R \sim 0.33$ mm

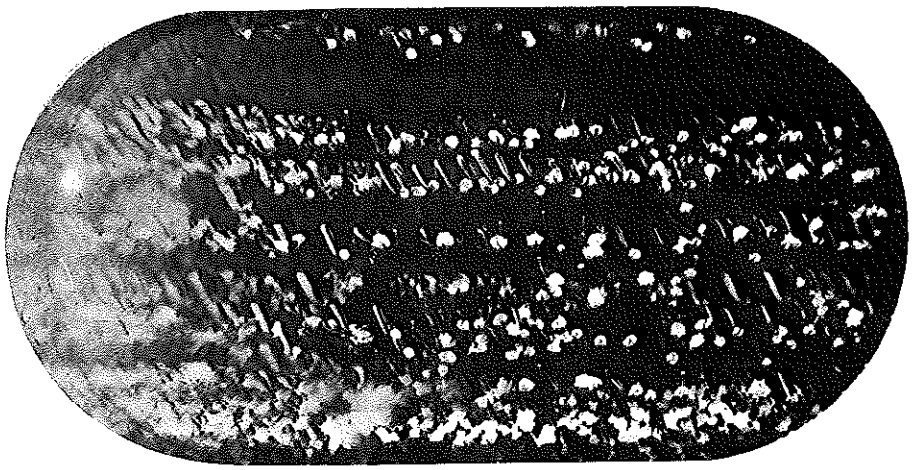

Heavy distortion of upper track; shorter displacement of its bubbles downwards

Change in the direction of the bubble movement

Explosion of track bubbles in the heat field of a neighboured track

Fig. 12a $\Delta t = 25$ ms, $R \sim 0.32$ mm

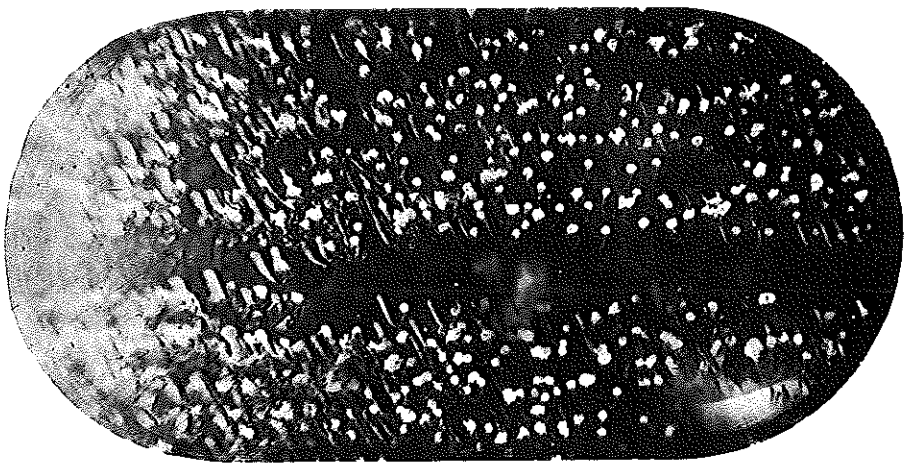

Fig. 13a Δt = 30 ms, R ~ 0.32 mm

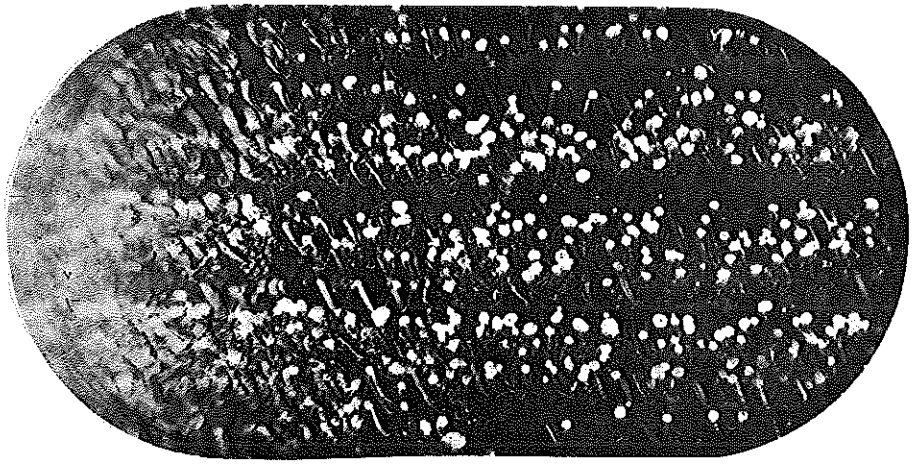

Identification of bubbles, which belonged to one and the same track, is no longer possible

Fig. 14a Δt = 35 ms, R ~ 0.32 mm

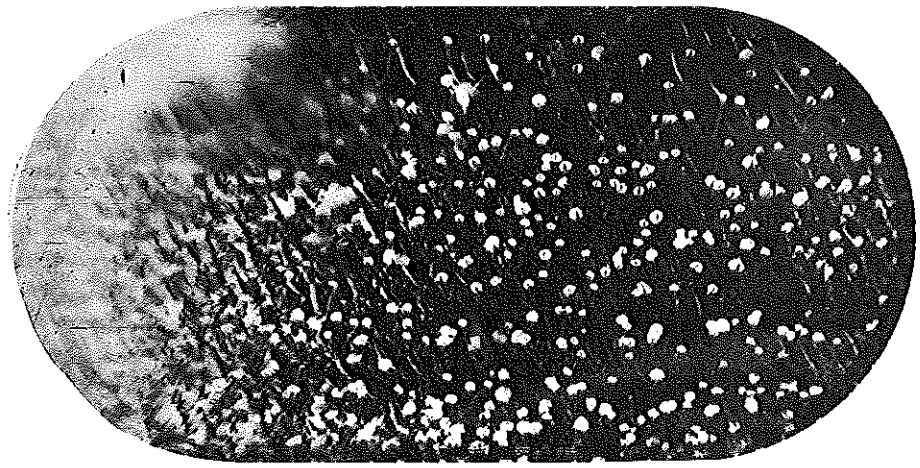

Fig. 15a Δt = 40 ms, R ~ 0.30 mm

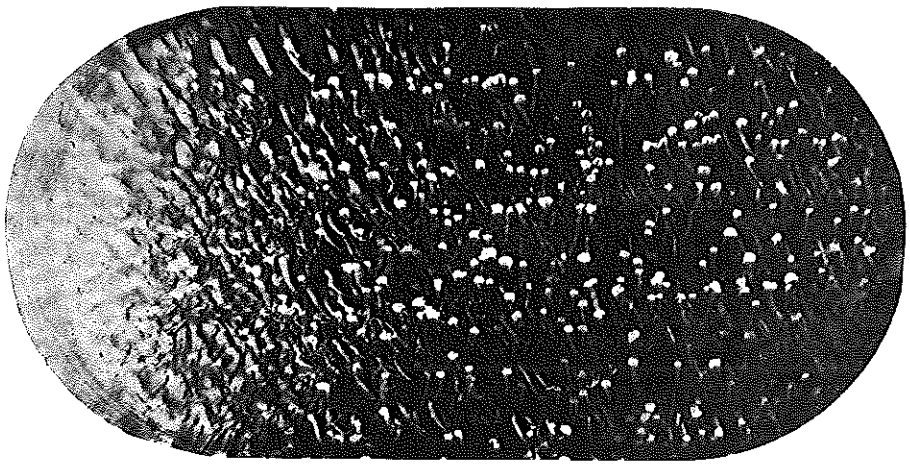

Figs. 4b - 15b $T = 25$ K

$P_v = 3.34$ kp/cm^2

$P_s = 5.40$ kp/cm^2

$P_{min} = 1.35$ kp/cm^2

Fig. 4b $\Delta t = 1$ ms, $R \sim 0.15$ mm, $b \sim 7$ bubbles/cm

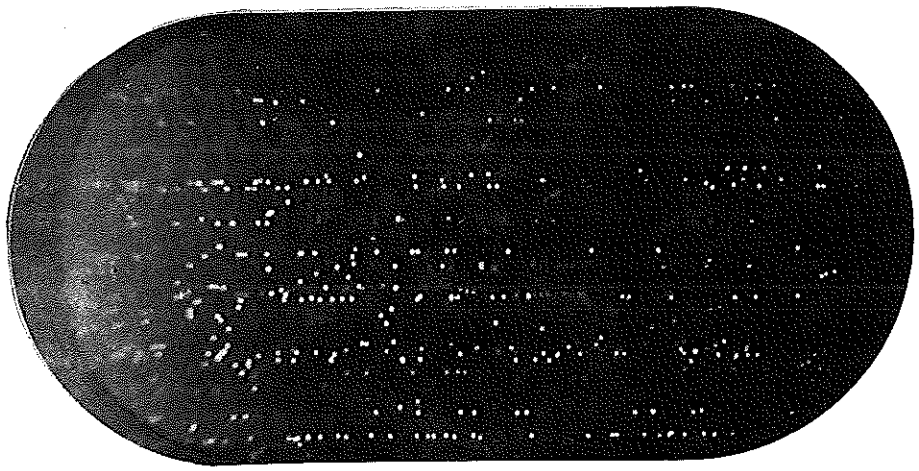

Spherical bubbles

Fig. 5b $\Delta t = 3$ ms, $R \sim 0.35$ mm, $b \sim 7$ bubbles/cm

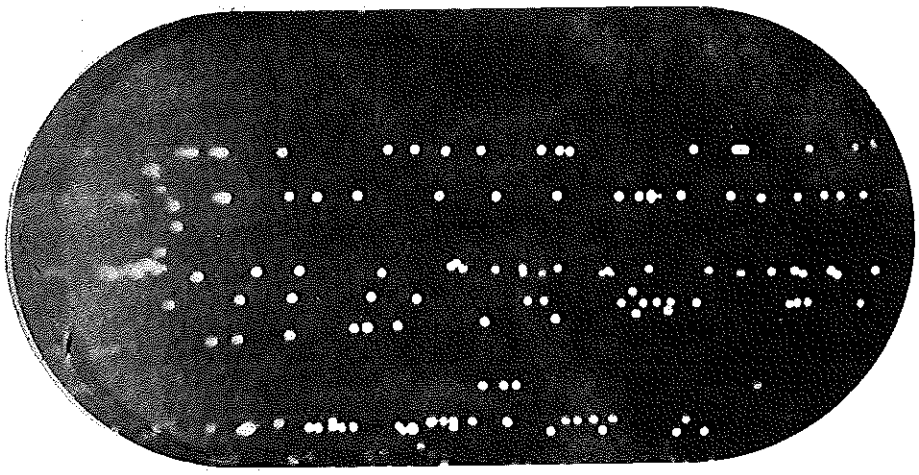

Fig. 6b $\Delta t = 5$ ms, $R \sim 0.43$ mm, $b \sim 6$ bubbles/cm

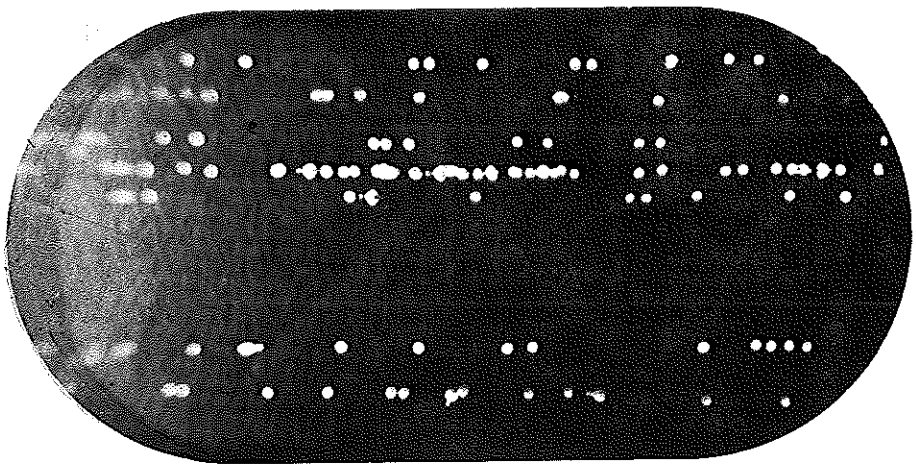

Bubble coalescence
Asymmetric deformation of some bubbles

Fig. 7b Δt = 7 ms, R$\sim$0.50 ms, b$\sim$5 bubbles/cm

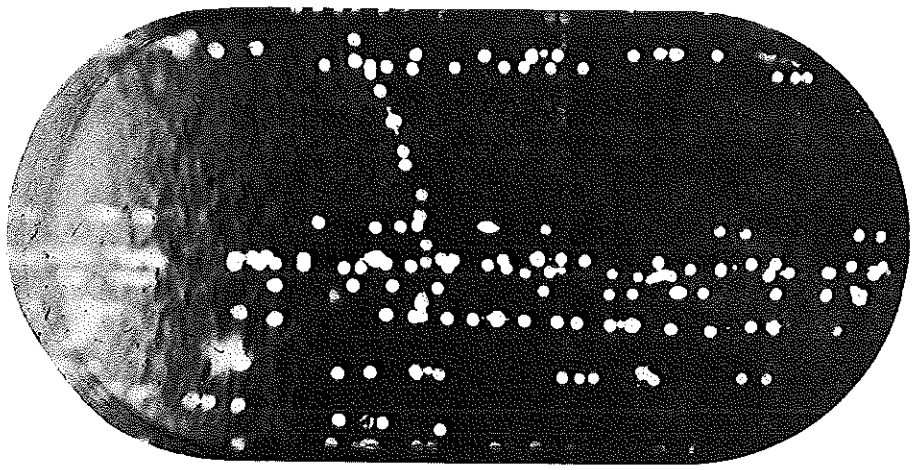

Fig. 8b Δt = 9 ms, R$\sim$0.48 ms, b$\sim$4 bubbles/cm

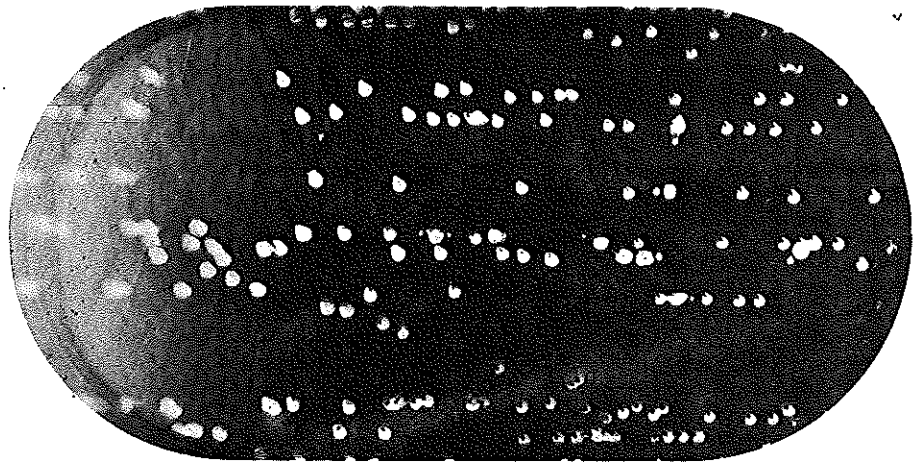

Fig. 9b Δt = 10 ms, R$\sim$0.45 mm, b$\sim$4 bubbles/cm

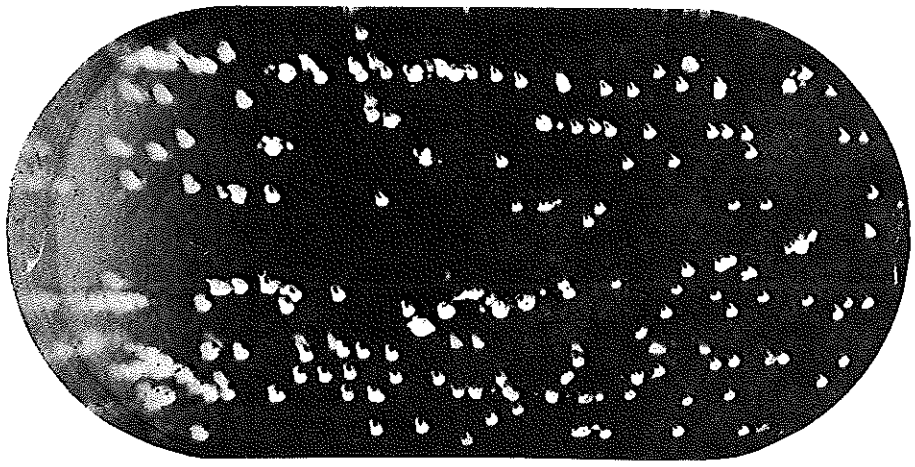

Schlieren-tail development is already visible

Fig. 10b Δt = 15 ms, $R \sim 0.34$ mm

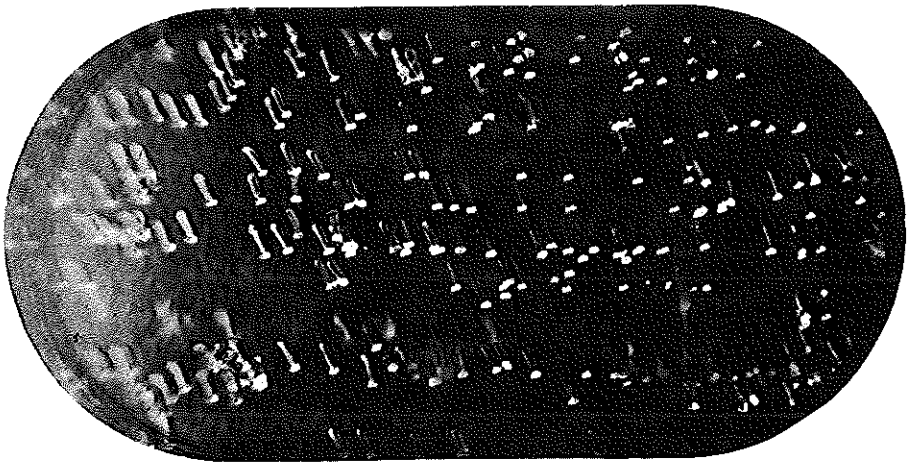

Fig. 11b Δt = 20 ms, $R \sim 0.35$ mm

Bubble "explosion"

Change in the direction of the movement

Fig. 12b Δt = 25 ms, $R \sim 0.30$ mm

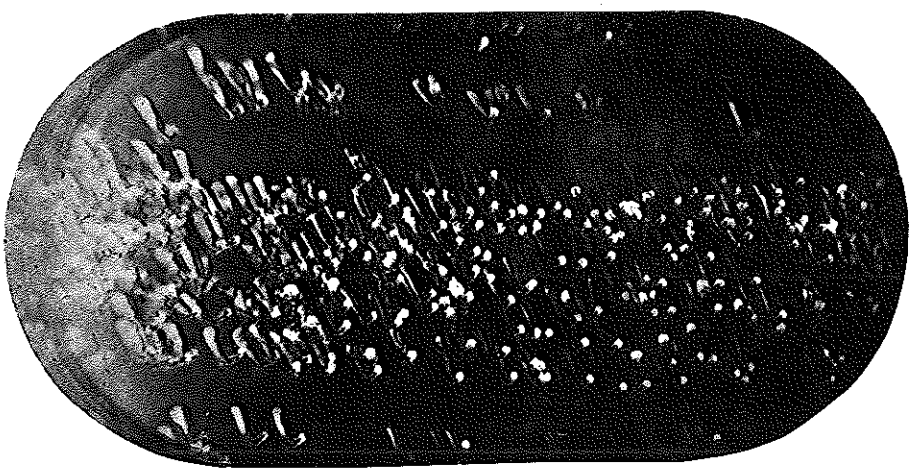

Bubbles begin to rise

Fig. 13b Δt = 30 ms, R~0.28 mm

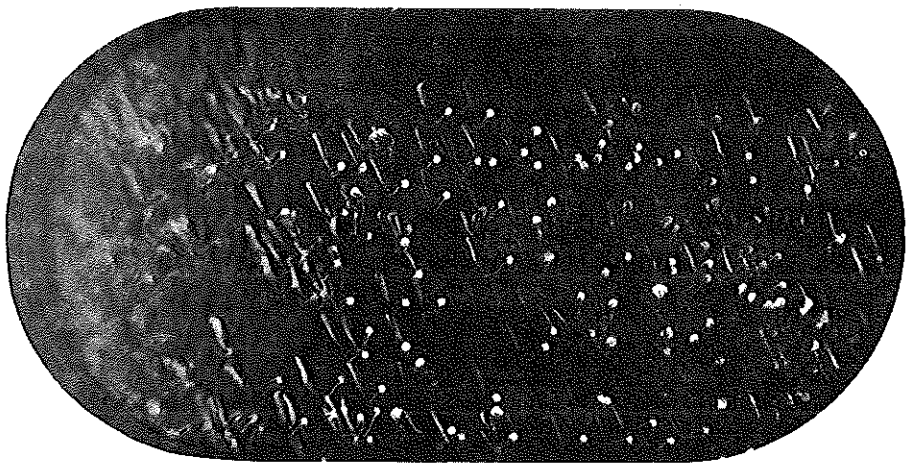

Fig. 14b Δt = 35 ms, R~0.27 mm

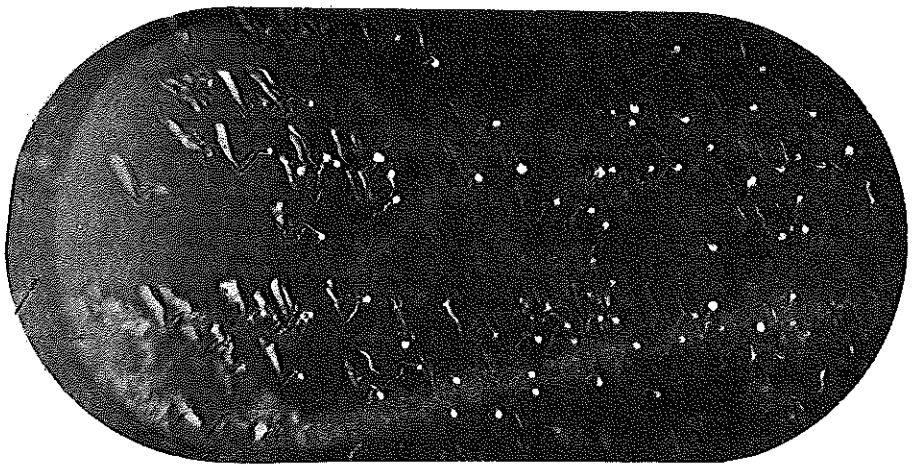

Influence of pressure on the direction of movement. This is irregular for different regions.

Fig. 15b Δt = 40 ms, R~0.20 mm

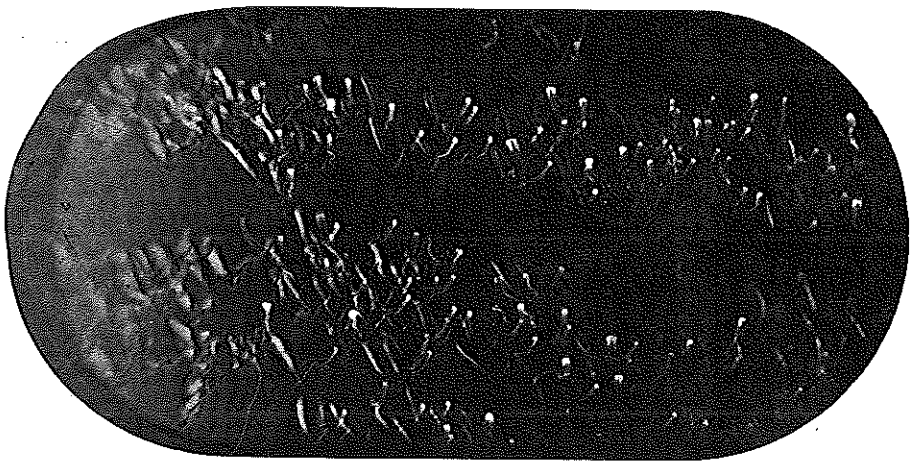

Bubbles change again the direction of their movement and rise.

Figs. 16 - 19 $T = 25$ K

$P_v = 3.34$ kp/cm^2

$P_s = 3.90$ kp/cm^2

$P_{min} = 1.25$ kp/cm^2

Fig. 16 $\Delta t = 1$ ms (small, dark bubble images)
R$\sim$0.20 mm, b$\sim$9 bubbles/cm

$\Delta t = 6$ ms (large, light bubble images)
R$\sim$0.48 mm, b$\sim$7 bubbles/cm

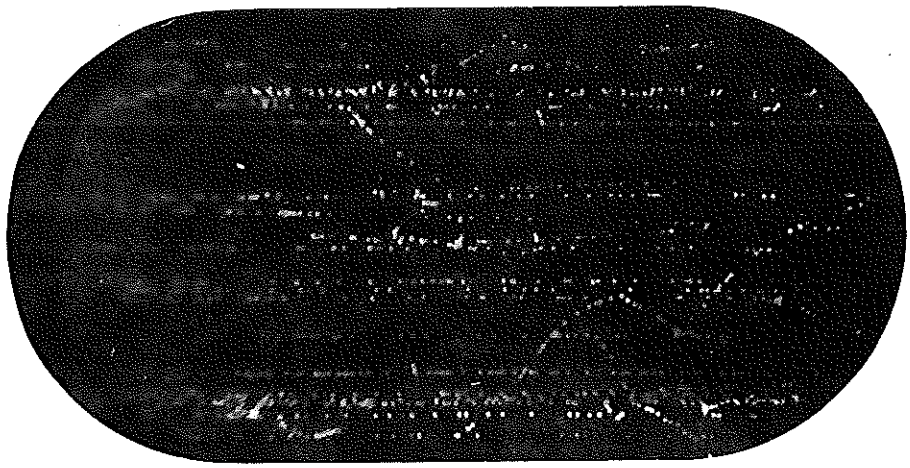

Irregular, small displacement with time of bubbles from original trajectory in different directions essentially downwards to the right

Fig. 17 $\Delta t = 6$ ms (large, dark bubble images)
R$\sim$0.48 mm, b$\sim$7 bubbles/cm

$\Delta t = 11$ ms (small, light bubbles images)
R$\sim$0.39 mm, b$\sim$7 bubbles/cm

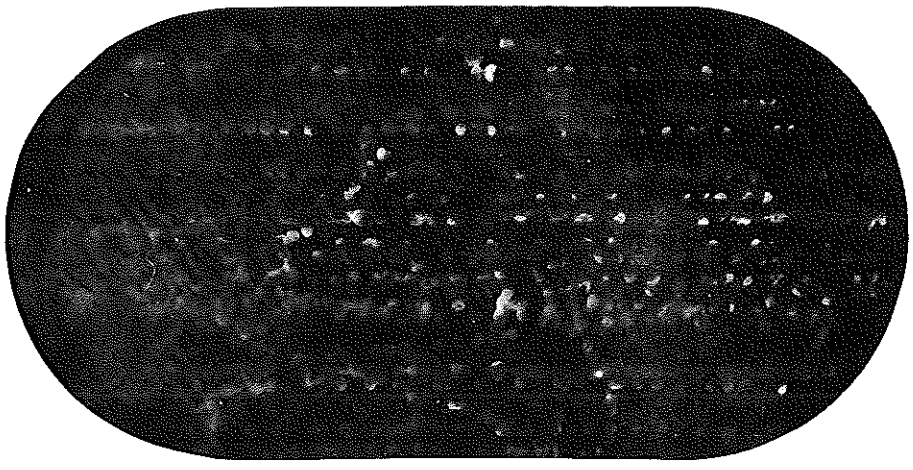

Displacement with time of all bubbles downwards to the right

Fig. 18 Δt = 11 ms (large, dark bubble images with good visible tail)
R~0.39 mm

Δt = 16 ms (small, light bubble images with no visible tail)
R~0.36 mm

Displacement with time of all bubbles downwards to the right

Fig. 19 Δt = 16 ms (large, dark bubble images with good visible tail)
R~0.36 mm

Δt = 21 ms (large, light bubble images with no visible tail)
R~0.33 mm

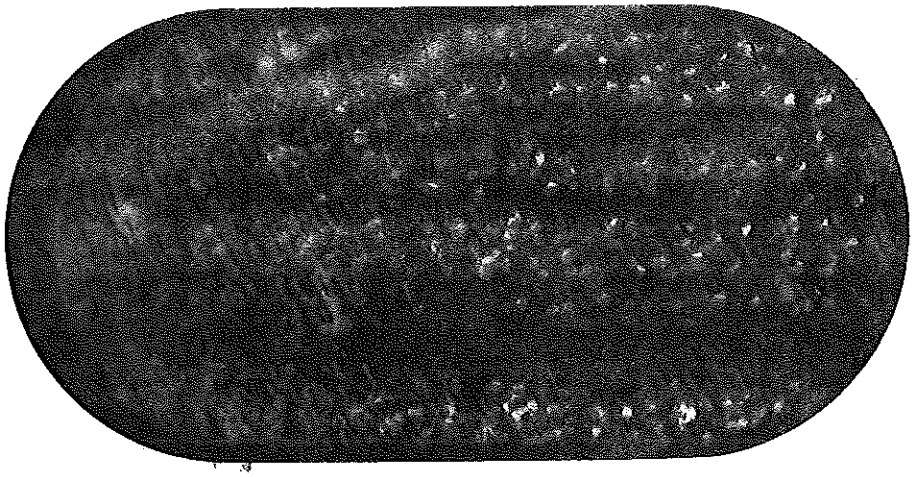

Small displacement with time of all bubbles upwards and essentially to the right

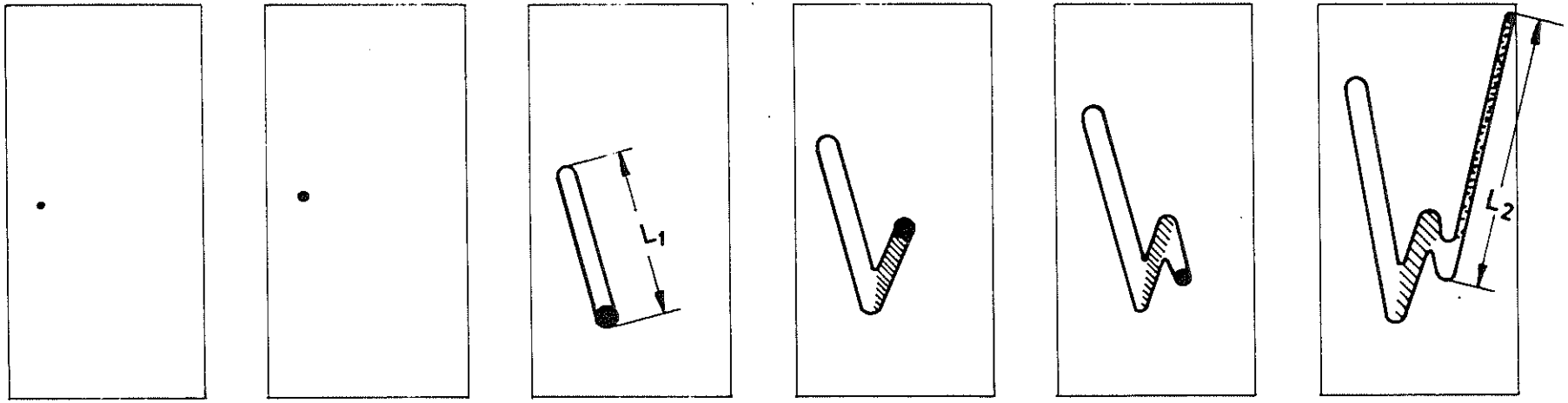

⓪ $t = t_0$ ① $t = t_1$ ② $t = t_2$ ③ $t = t_3$ ④ $t = t_4$ ⑤ $t = t_5$

$\Delta t_1 = t_1 - t_0$

$\Delta t_2 = t_2 - t_1$

$\Delta t_3 = t_4 - t_2$

$\Delta t_4 = t_5 - t_4$

Displacement of a bubble relative to the liquid (schematic)

Bubble

Schlieren tail, inertia forces dominating

Schlieren tail, bouyancy forces dominating

Schlieren tail due to buoyancy forces only

FIG. 20

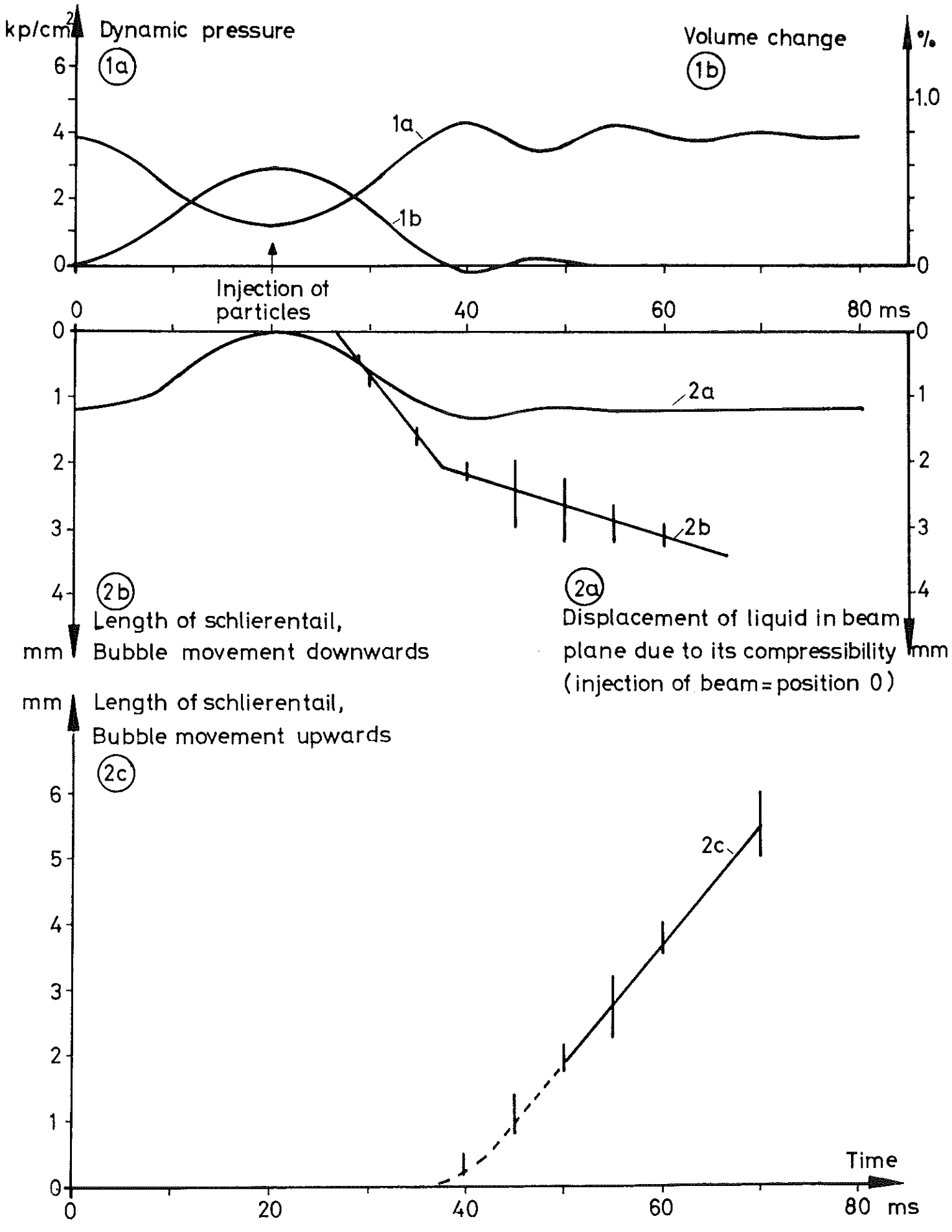

HYDROGEN: P_V = 3.34 kp/cm²
P_s = 3.90 kp/cm²
P_{min} = 1.25 kp/cm²

T ~ 25° K

FIG. 21/1

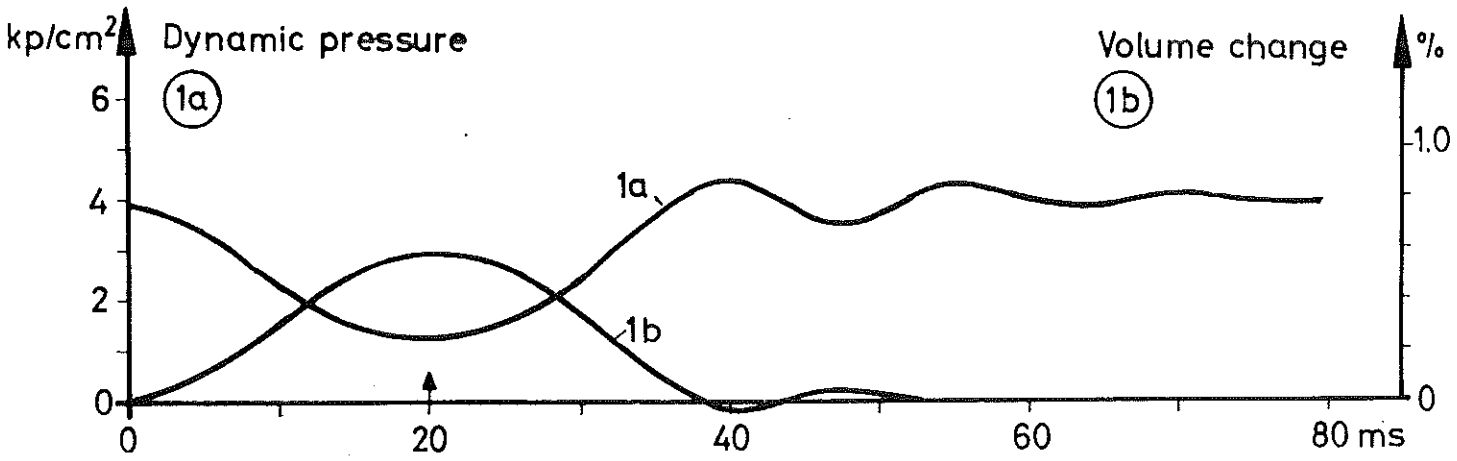

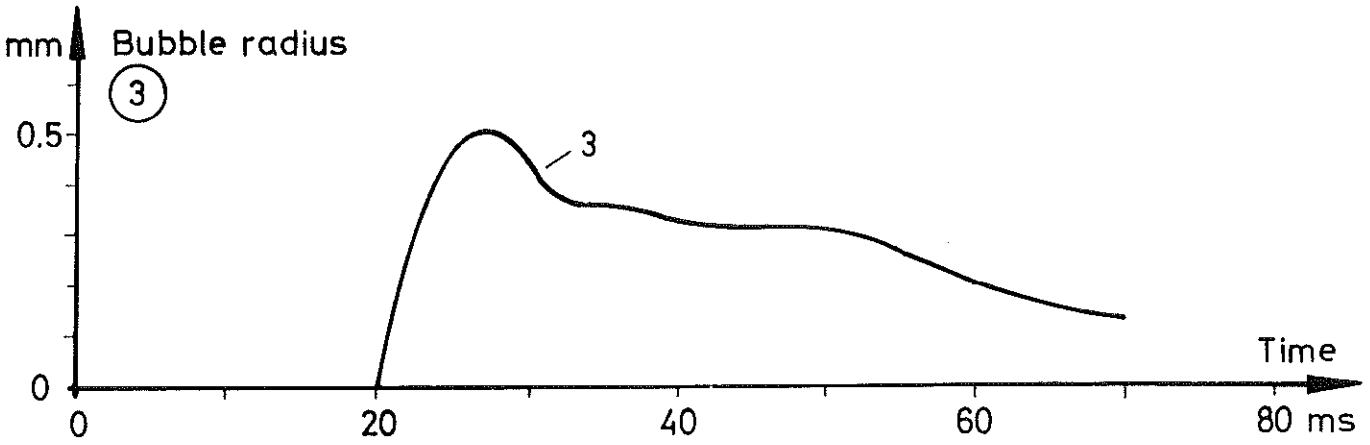

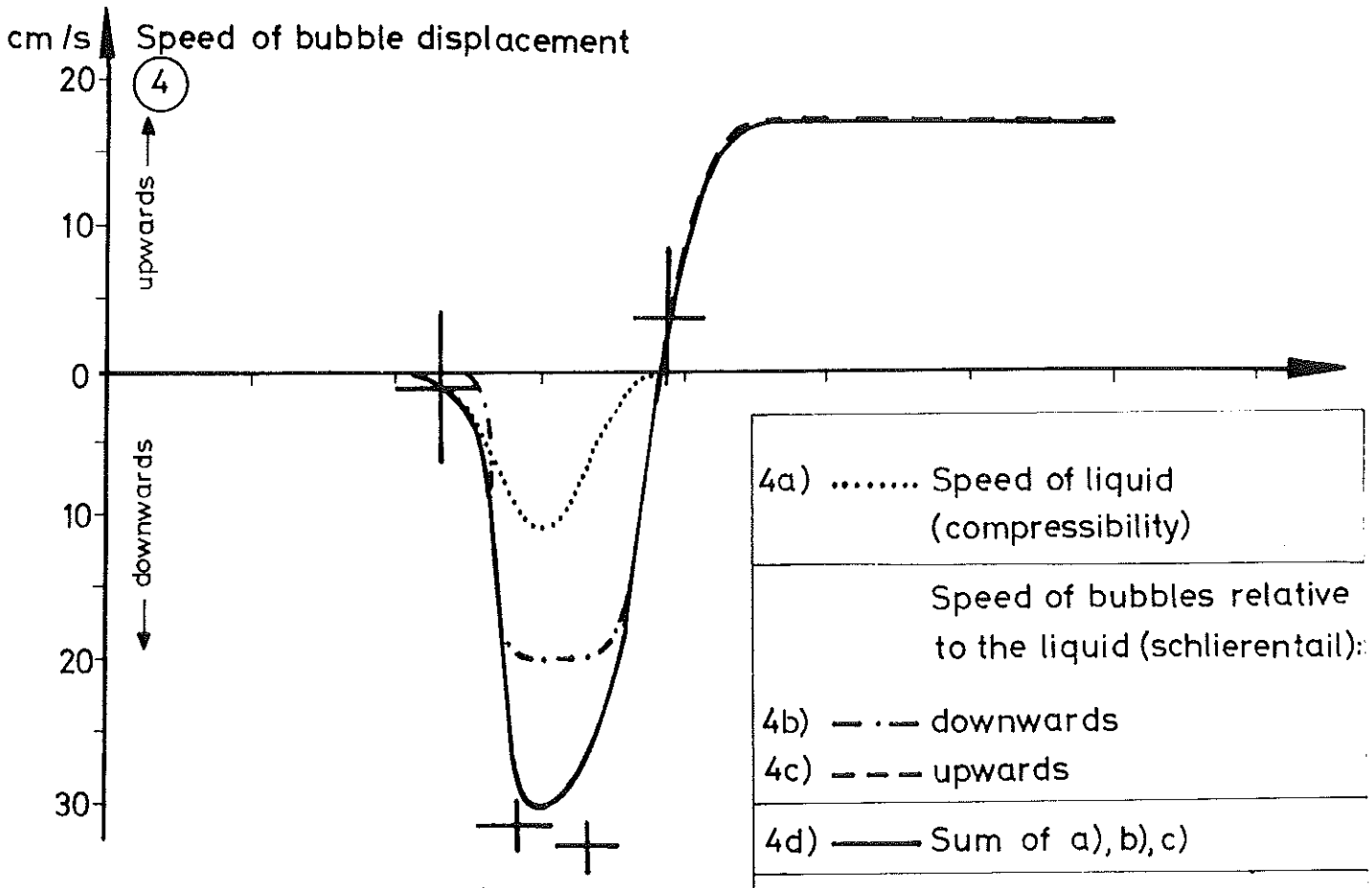

4a)	Speed of liquid (compressibility)
	Speed of bubbles relative to the liquid (schlierentail):
4b) — · —	downwards
4c) — — —	upwards
4d) ———	Sum of a), b), c)
4e) +	Speed of total bubble displacement (double flash)

HYDROGEN: $T \sim 25^{\circ}K$, $P_v = 3.34$ kp/cm², $P_s = 3.90$ kp/cm², $P_{min} = 1.25$ kp/cm²

FIG. 21/2

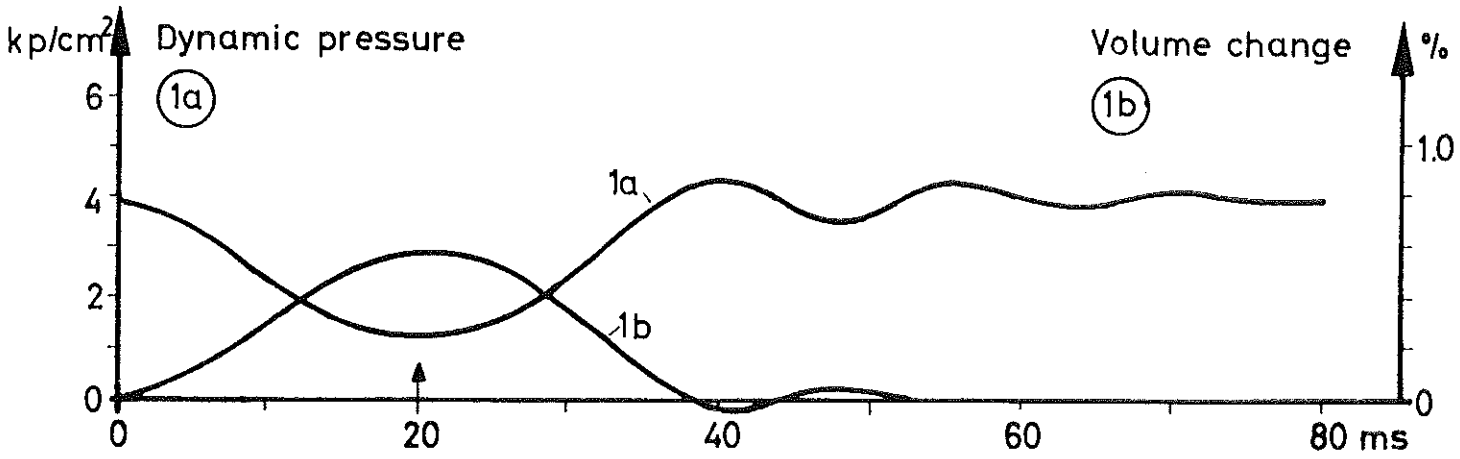

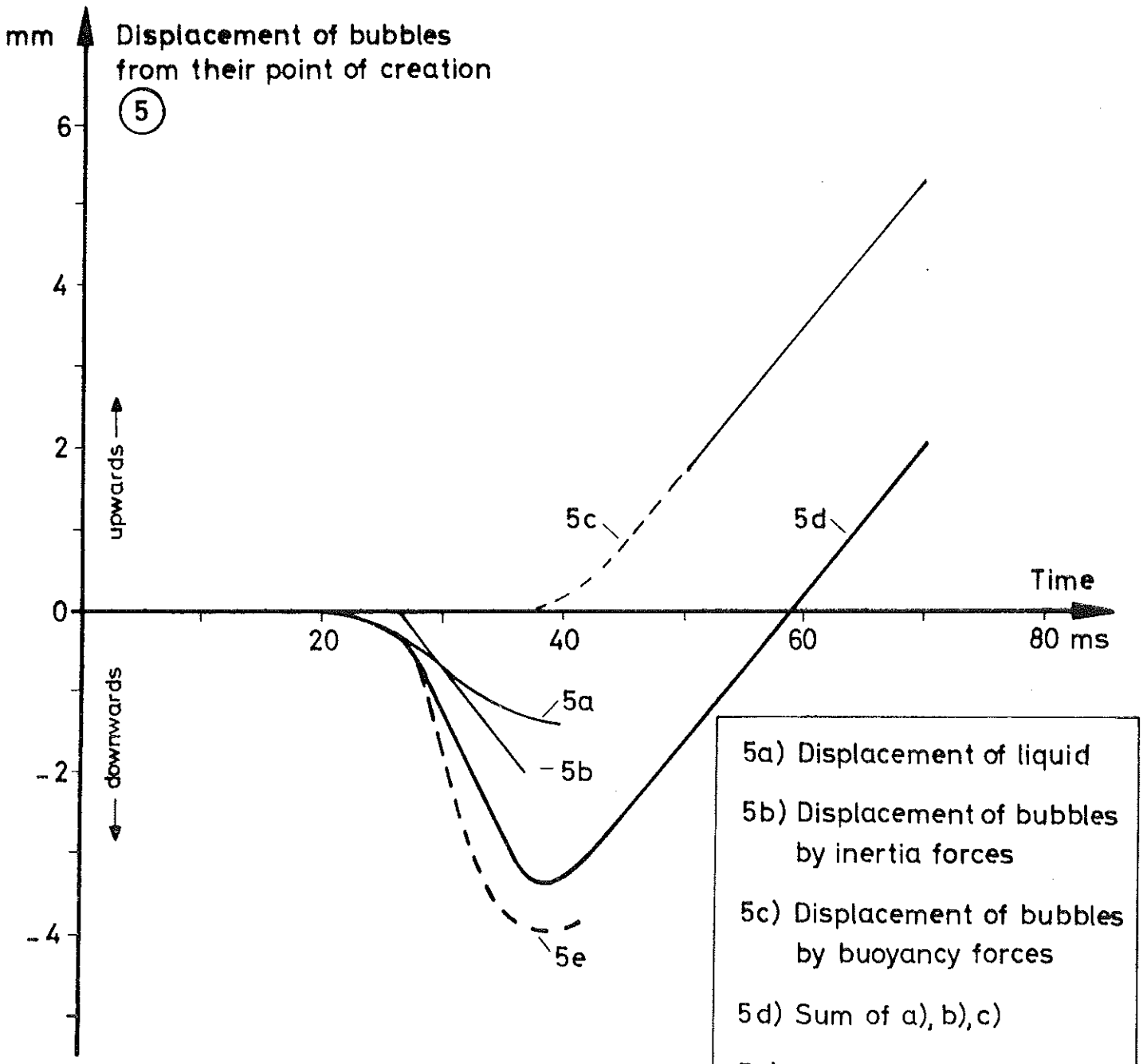

5a) Displacement of liquid

5b) Displacement of bubbles by inertia forces

5c) Displacement of bubbles by buoyancy forces

5d) Sum of a), b), c)

5e) Measured total displacement (double flash)

HYDROGEN: $T \sim 25°\ K$, $P_v = 3.34\ kp/cm^2$, $P_s = 3.90\ kp/cm^2$, $P_{min} = 1.25\ kp/cm^2$

FIG. 21/3

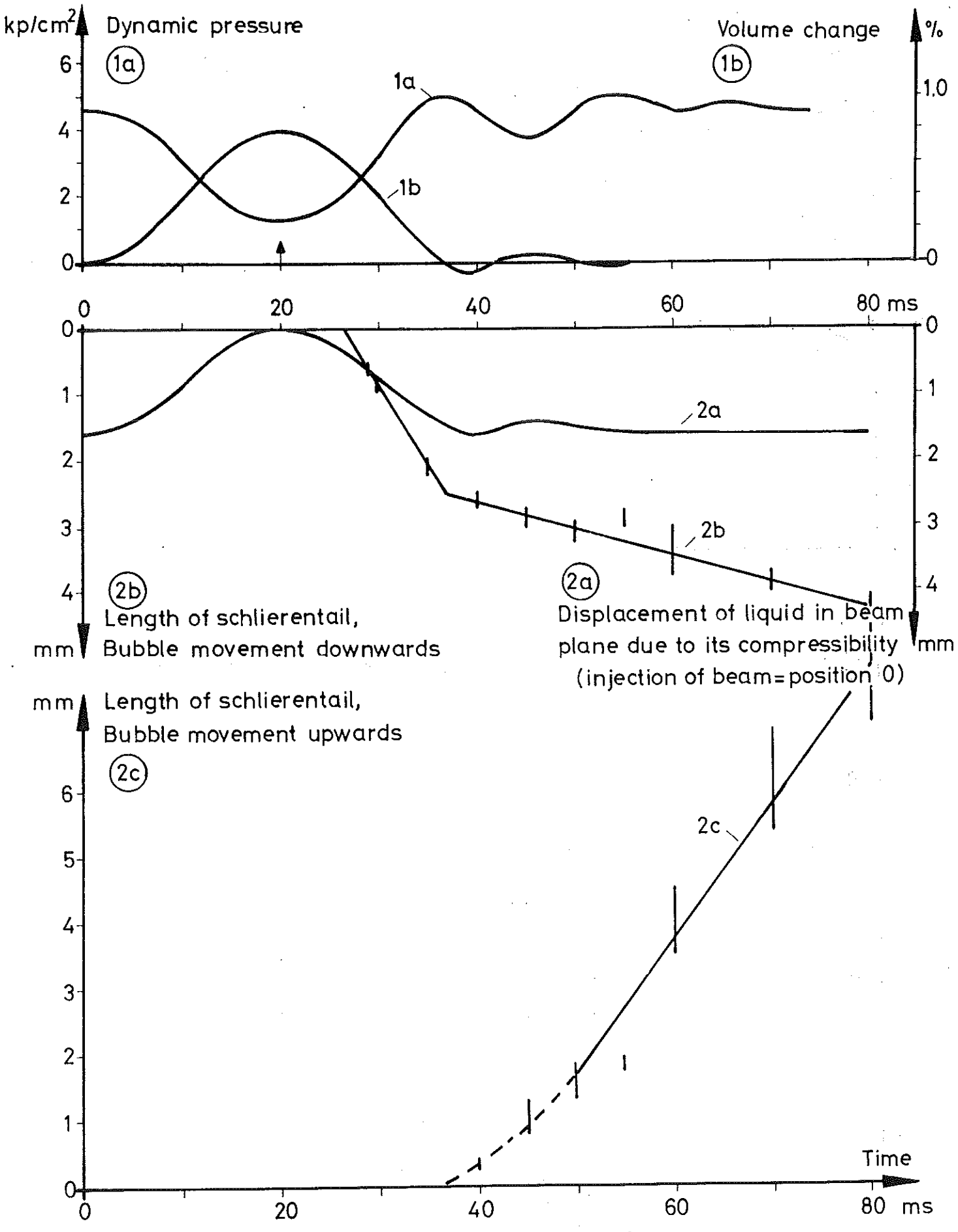

HYDROGEN: P_v = 3.34 kp/cm²
P_s = 4.60 kp/cm²
P_{min} = 1.25 kp/cm²

T ~ 25° K

FIG. 22/1

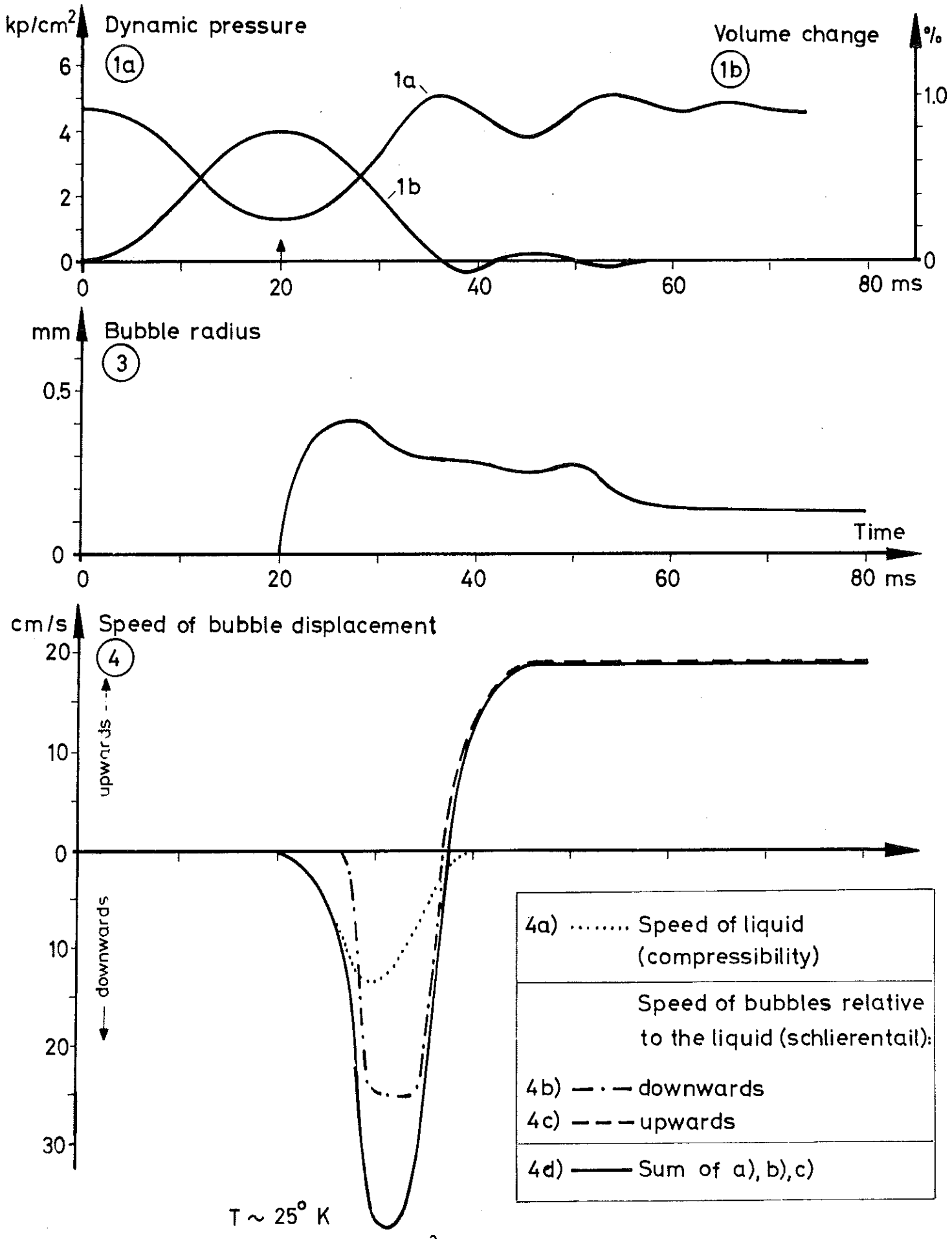
kp/cm²
Dynamic pressure
1a
6
4
2
0
1a
1b
Volume change
1b
%
1.0
0
0
20
40
60
80 ms
mm
Bubble radius
3
0.5
0
Time
0
20
40
60
80 ms
cm/s
Speed of bubble displacement
4
20
10
0
upwards
downwards
10
20
30
4a) ..... Speed of liquid (compressibility)
Speed of bubbles relative to the liquid (schlierentail):
4b) —·— downwards
4c) — — — upwards
4d) —— Sum of a), b), c)
T ~ 25° K
HYDROGEN: P_v = 3.34 kp/cm²
P_s = 4.60 kp/cm²
P_{min} = 1.25 kp/cm²

FIG. 22/2

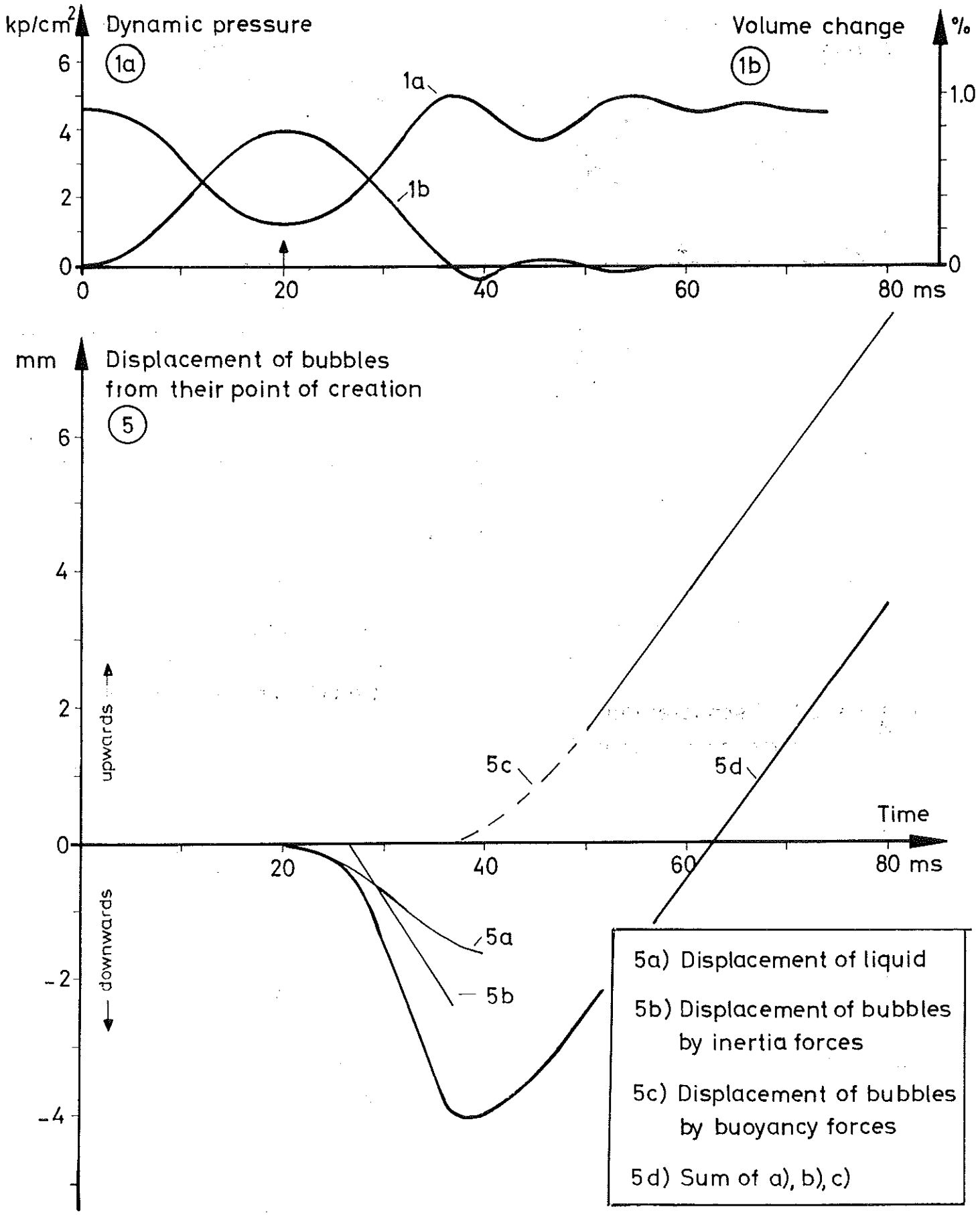

HYDROGEN: $T \sim 25^\circ K$

$P_v = 3.34$ kp/cm²

$P_s = 4.60$ kp/cm²

$P_{min} = 1.25$ kp/cm²

FIG. 22/3

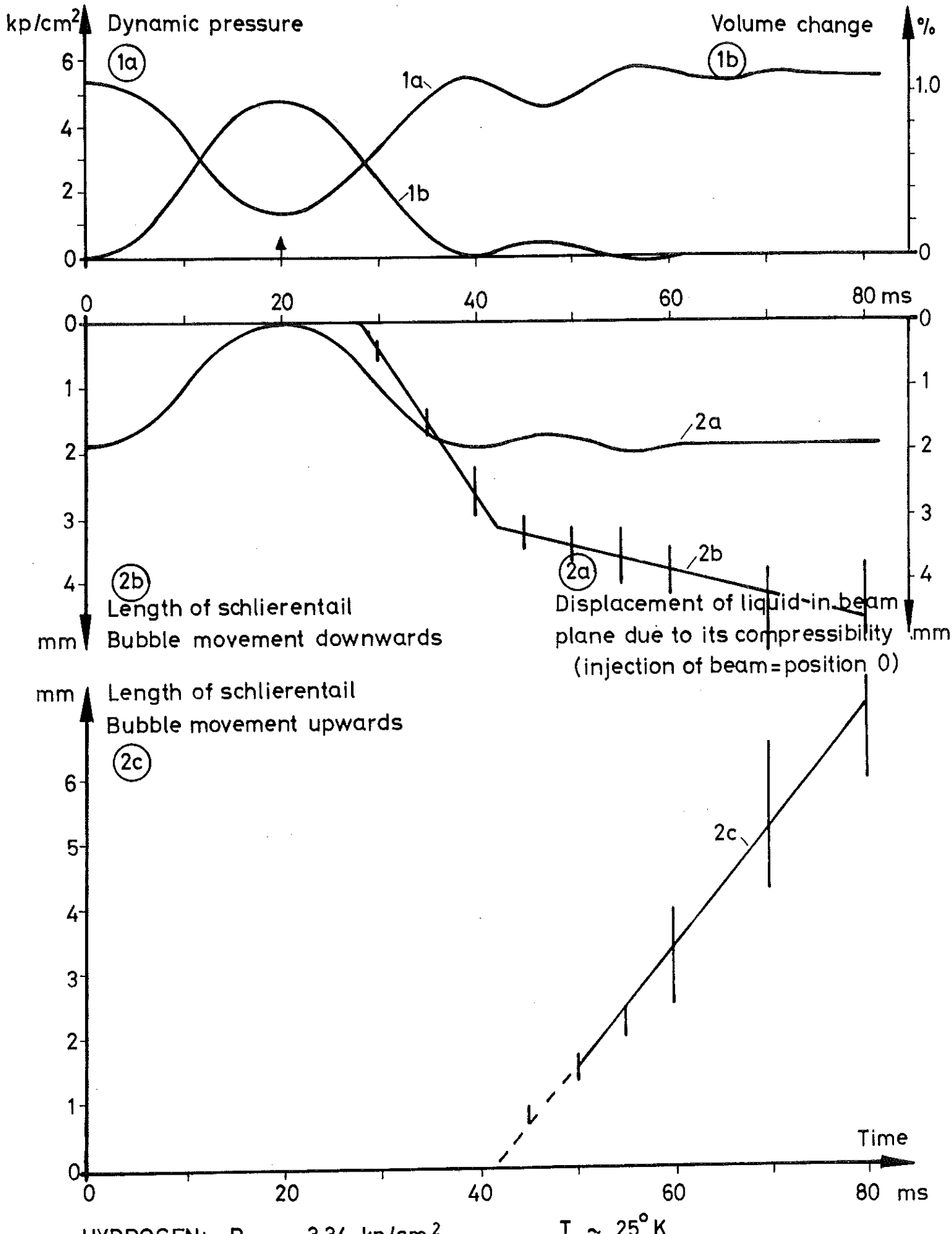
kp/cm²
Dynamic pressure
Volume change
%
1a
1b
1.0
0
2
4
6
0
20
40
60
80 ms
2a
2b
mm
Length of schlierentail
Bubble movement downwards
Displacement of liquid-in-beam plane due to its compressibility
(injection of beam = position 0)
Length of schlierentail
Bubble movement upwards
2c
Time
HYDROGEN: P_v = 3.34 kp/cm²
P_s = 5.40 kp/cm²
P_{min} = 1.35 kp/cm²
T ~ 25° K

FIG. 23/1

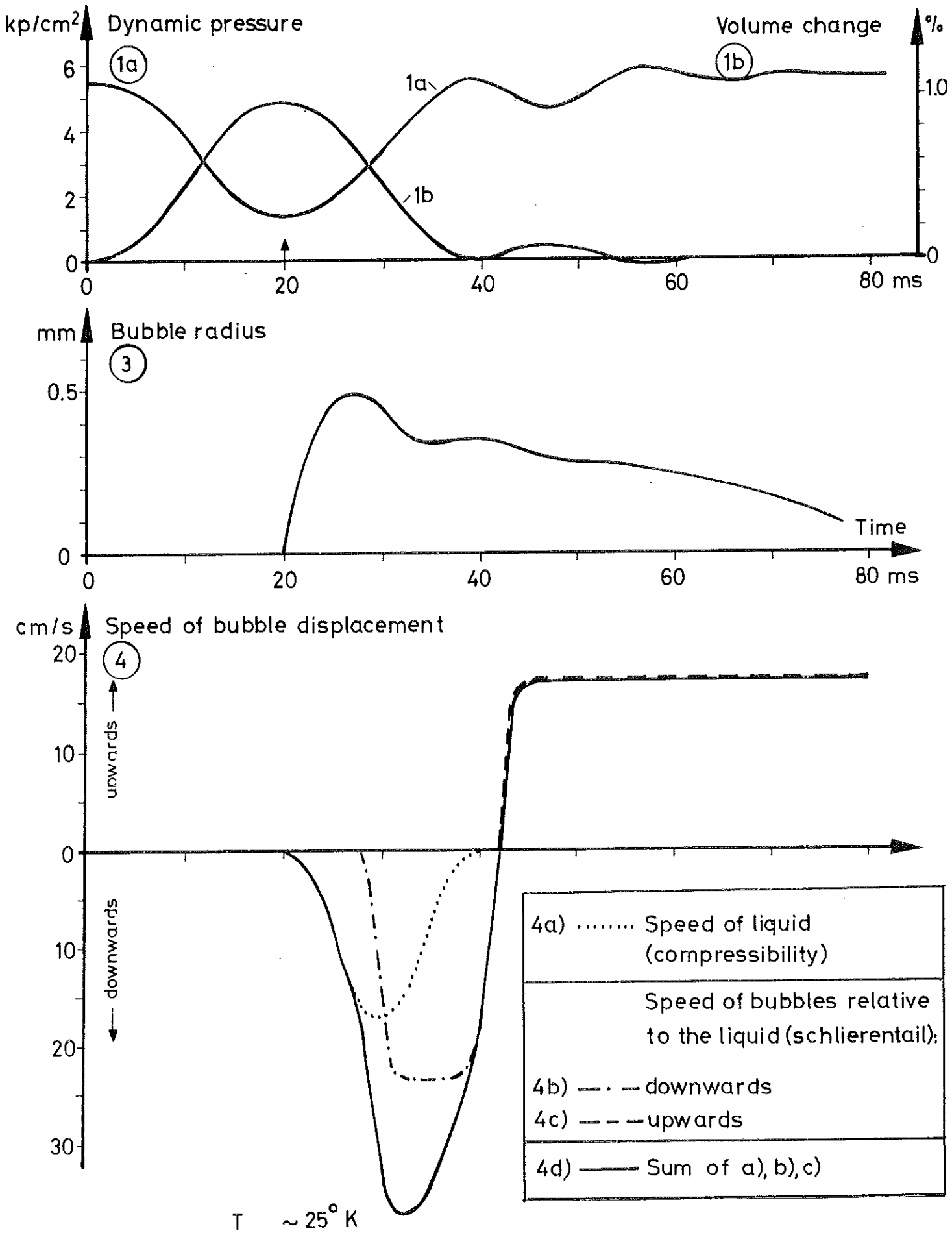

HYDROGEN: T ~ 25° K
P_v = 3.34 kp/cm²
P_s = 5.40 kp/cm²
P_{min} = 1.35 kp/cm²

FIG. 23 / 2

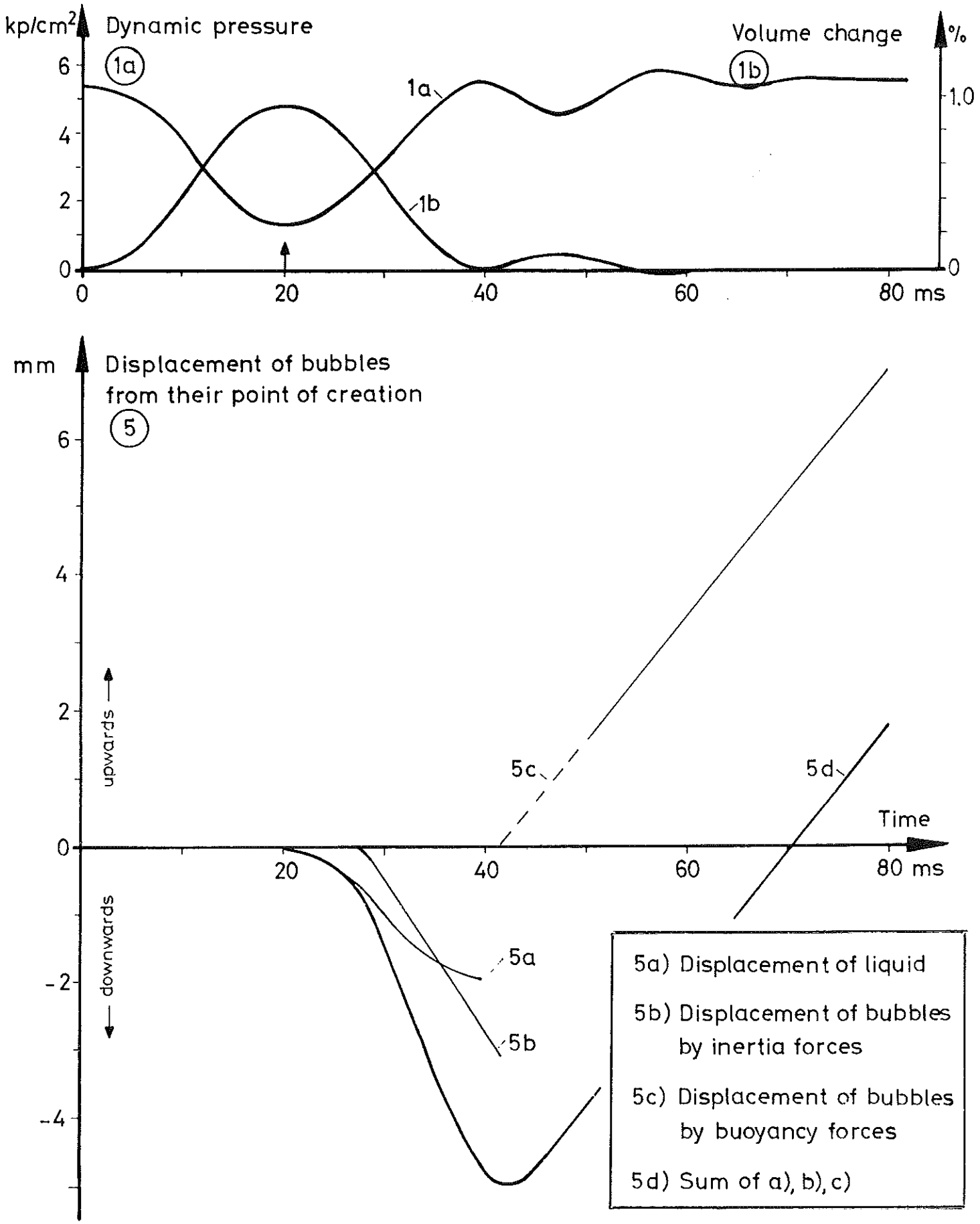

HYDROGEN: $T \sim 25^\circ K$, $P_v = 3.34$ kp/cm², $P_s = 5.40$ kp/cm², $P_{min} = 1.35$ kp/cm²

FIG. 23/3

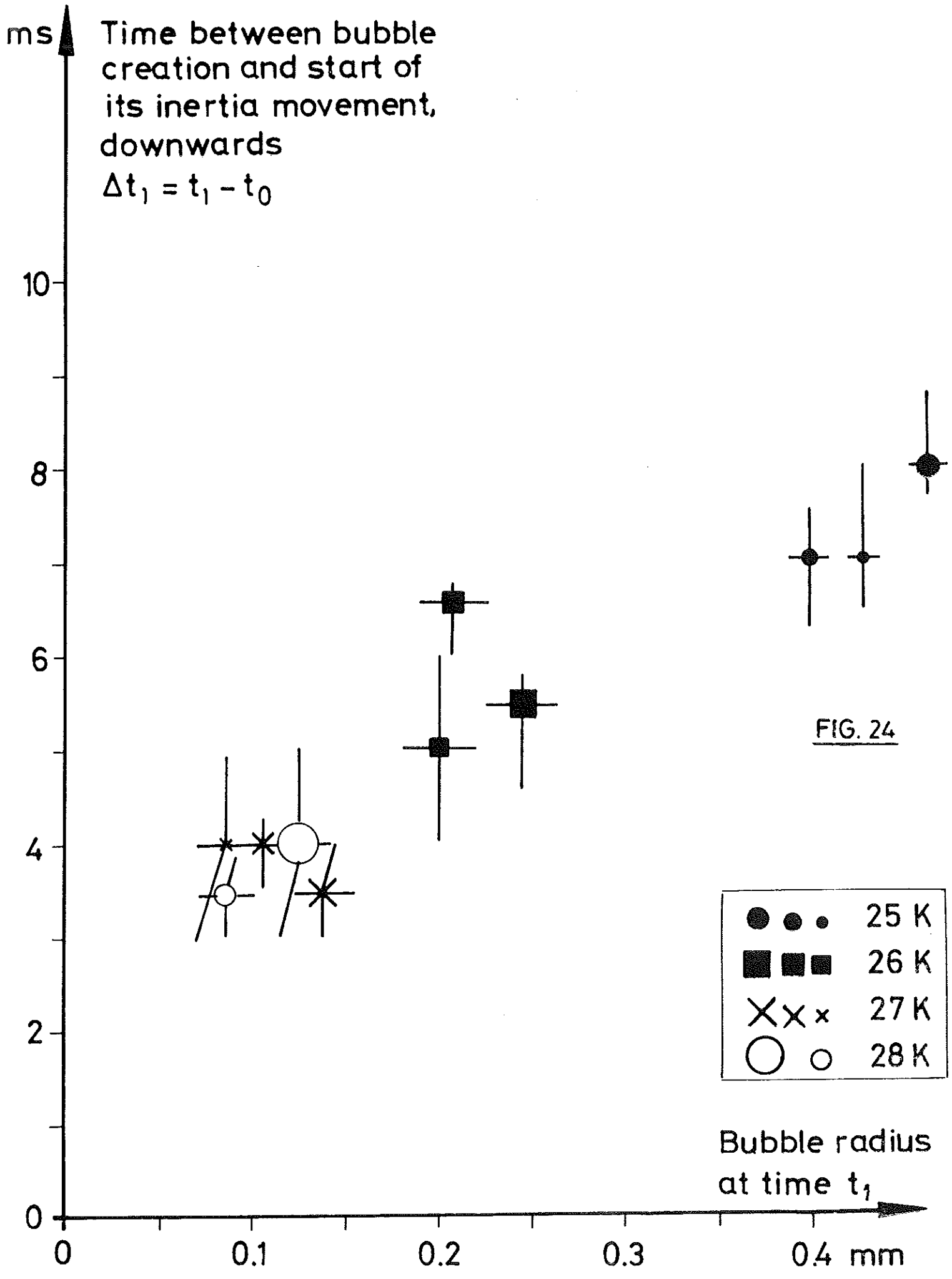
ms
Time between bubble creation and start of its inertia movement, downwards
$\Delta t_1 = t_1 - t_0$
10
8
6
4
2
0
0
0.1
0.2
0.3
0.4 mm
Bubble radius at time t_1
25 K
26 K
27 K
28 K

FIG. 24

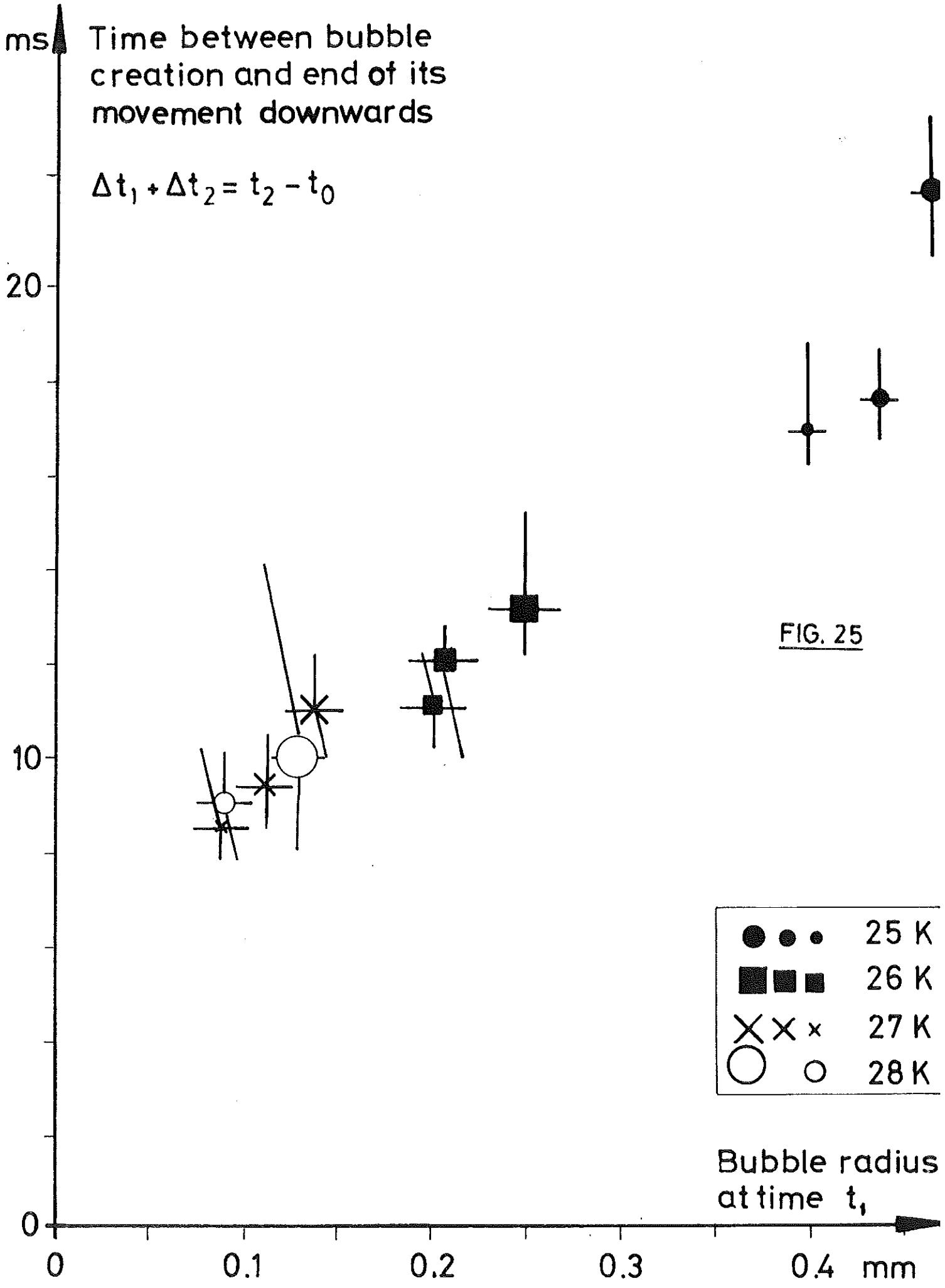
ms
Time between bubble creation and end of its movement downwards
$\Delta t_1 + \Delta t_2 = t_2 - t_0$
20
10
0
0
0.1
0.2
0.3
0.4 mm
25 K
26 K
27 K
28 K
Bubble radius at time t_1

FIG. 25

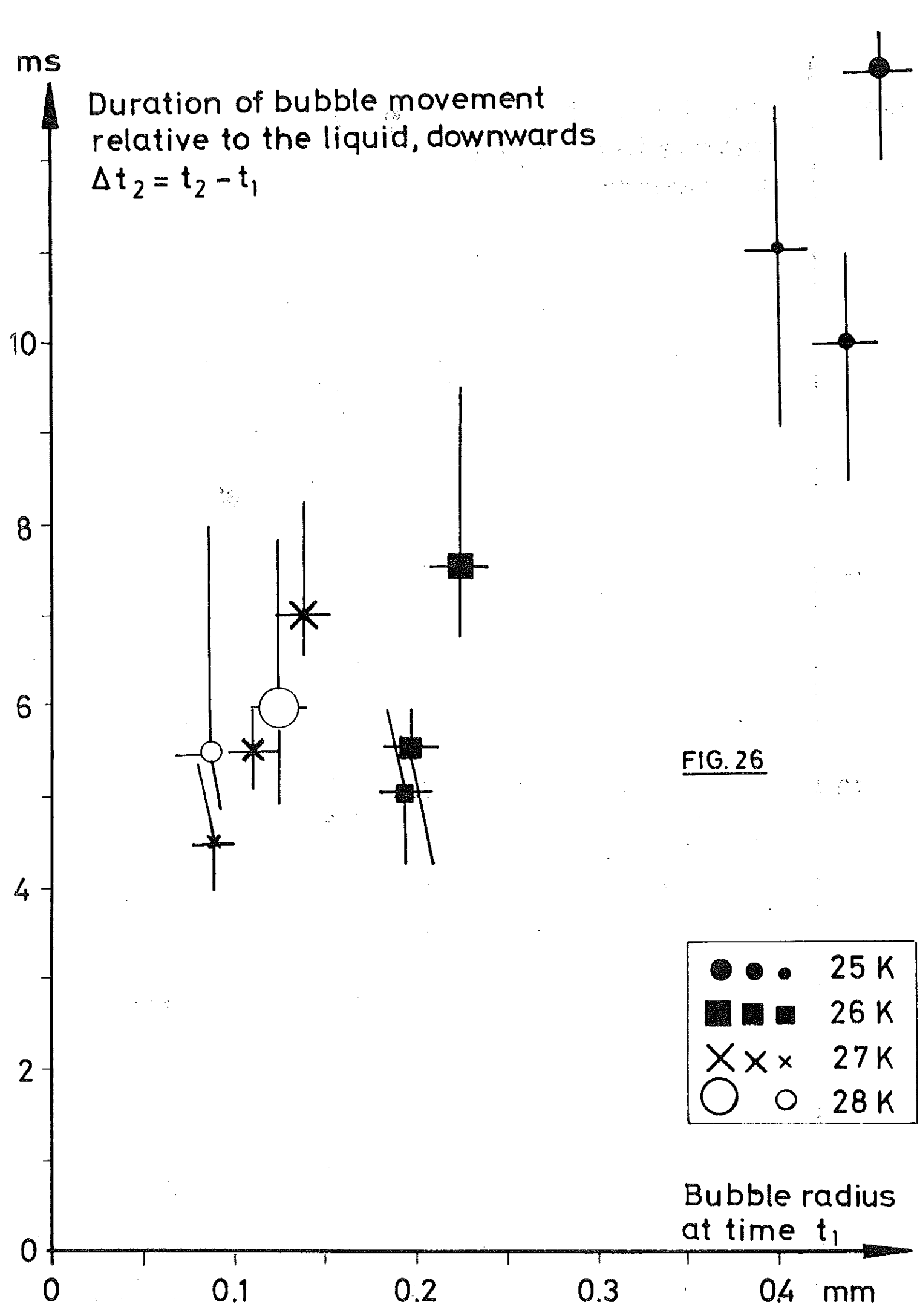
ms
Duration of bubble movement
relative to the liquid, downwards
$\Delta t_2 = t_2 - t_1$
10
8
6
4
2
0
0
0.1
0.2
0.3
0.4 mm
Bubble radius
at time t_1
25 K
26 K
27 K
28 K

FIG. 26

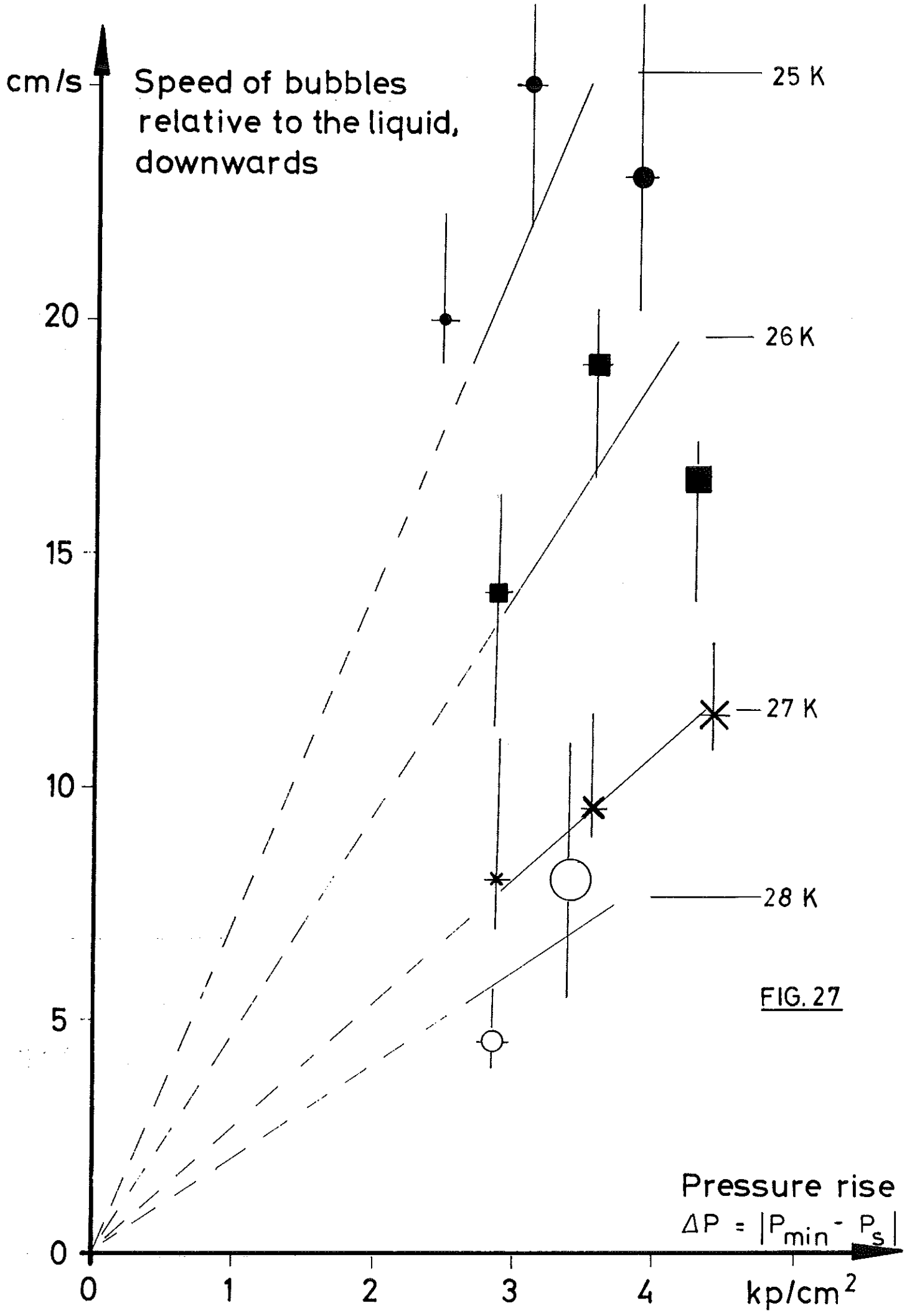
cm/s
Speed of bubbles relative to the liquid, downwards
25 K
26 K
27 K
28 K
20
15
10
5
0
0
1
2
3
4
kp/cm²
Pressure rise
ΔP = |P_min - P_s|

FIG. 27

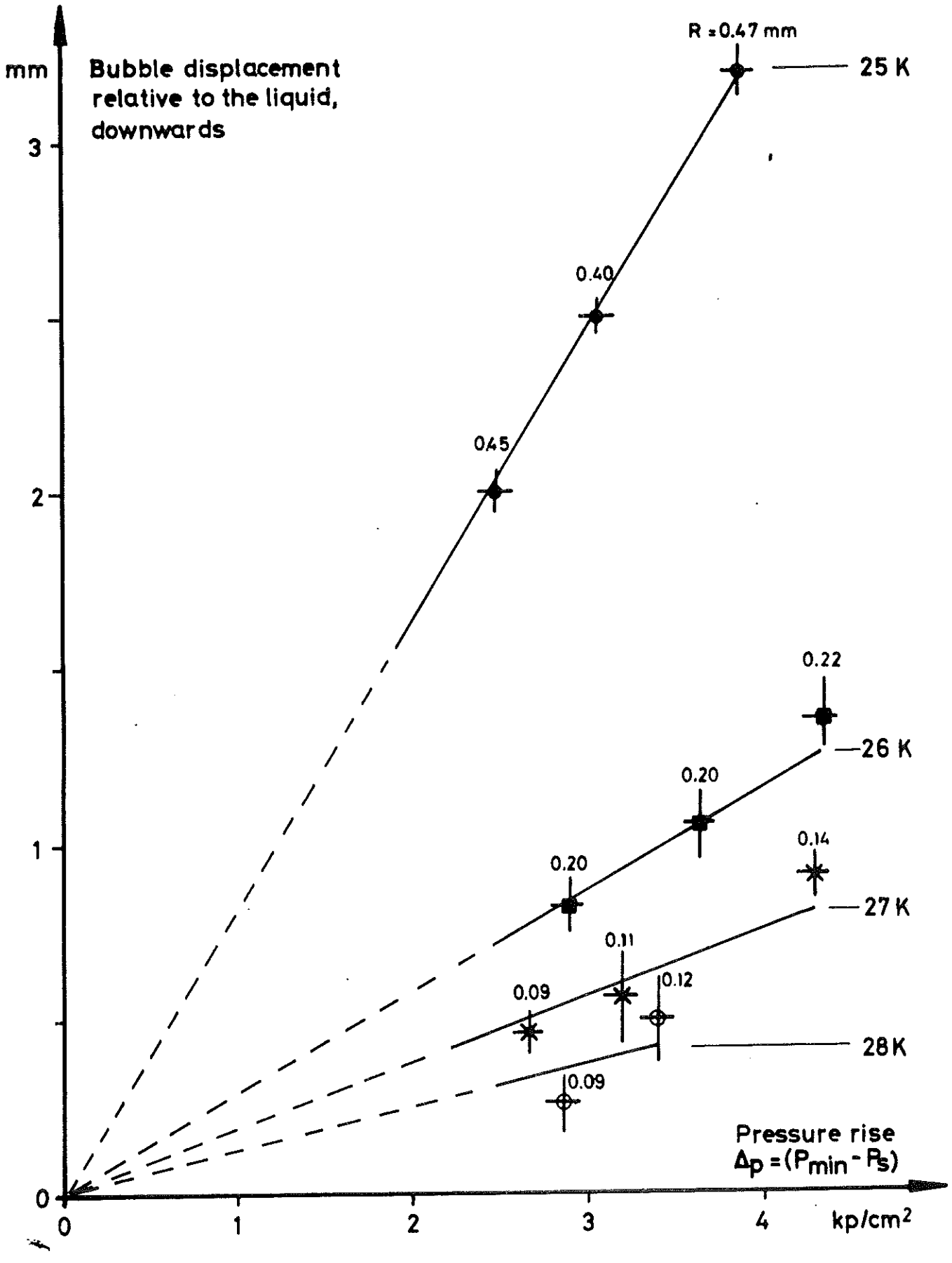
mm
Bubble displacement relative to the liquid, downwards
R = 0.47 mm
25 K
0.40
0.45
0.22
26 K
0.20
0.20
0.14
27 K
0.11
0.09
0.12
28 K
0.09
Pressure rise
Δp = (Pmin - Ps)
kp/cm²
0
1
2
3
4

FIG. 28

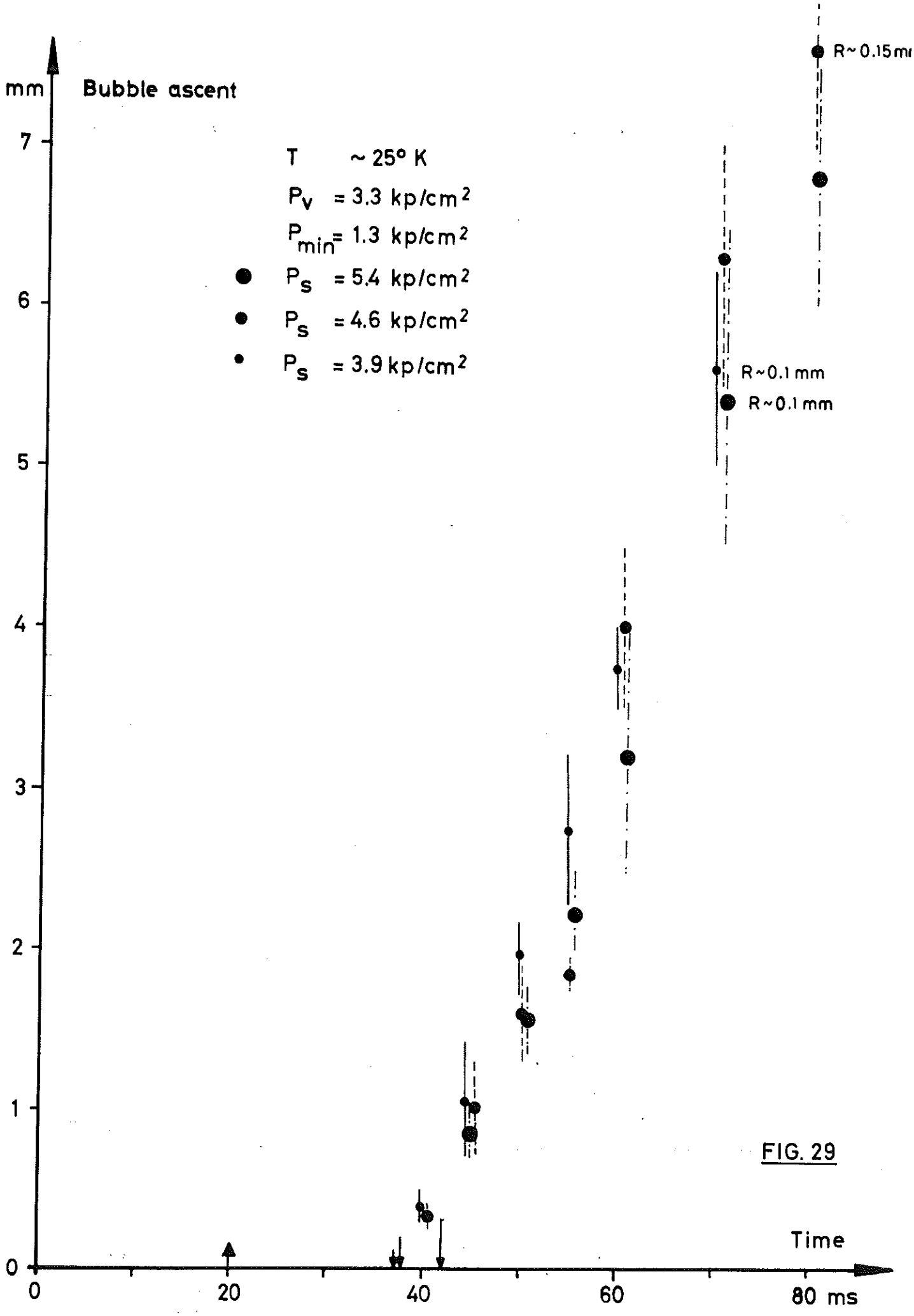
Bubble ascent
mm
T ~ 25° K
P_v = 3.3 kp/cm²
P_{min} = 1.3 kp/cm²
P_s = 5.4 kp/cm²
P_s = 4.6 kp/cm²
P_s = 3.9 kp/cm²
R~0.15m
R~0.1 mm
R~0.1 mm
7
6
5
4
3
2
1
0
0
20
40
60
80 ms
Time

FIG. 29

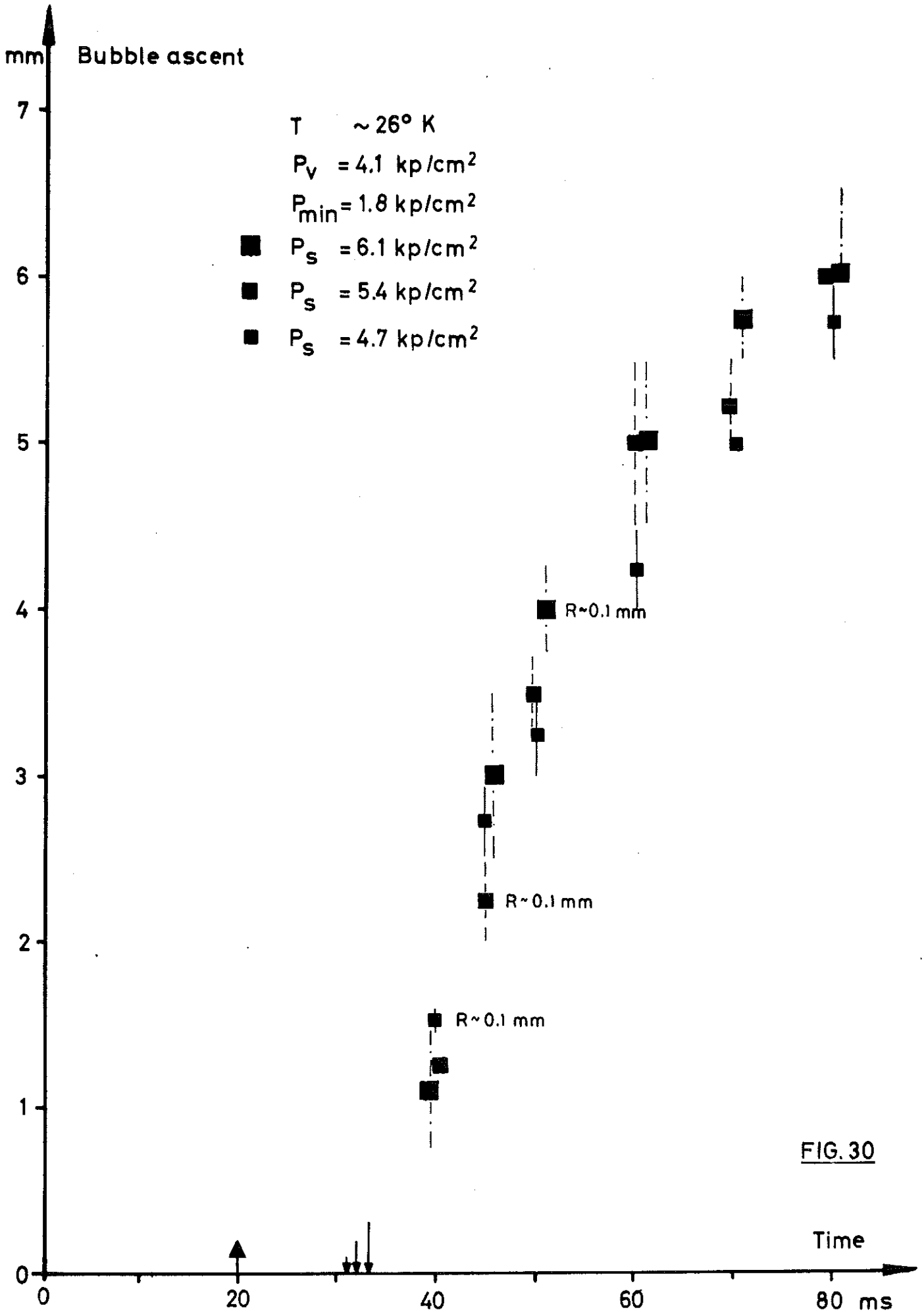
mm
Bubble ascent
7
6
5
4
3
2
1
0
T ~ 26° K
P_v = 4.1 kp/cm²
P_{min} = 1.8 kp/cm²
P_s = 6.1 kp/cm²
P_s = 5.4 kp/cm²
P_s = 4.7 kp/cm²
R~0.1 mm
R~0.1 mm
R~0.1 mm
Time
0
20
40
60
80 ms

FIG. 30

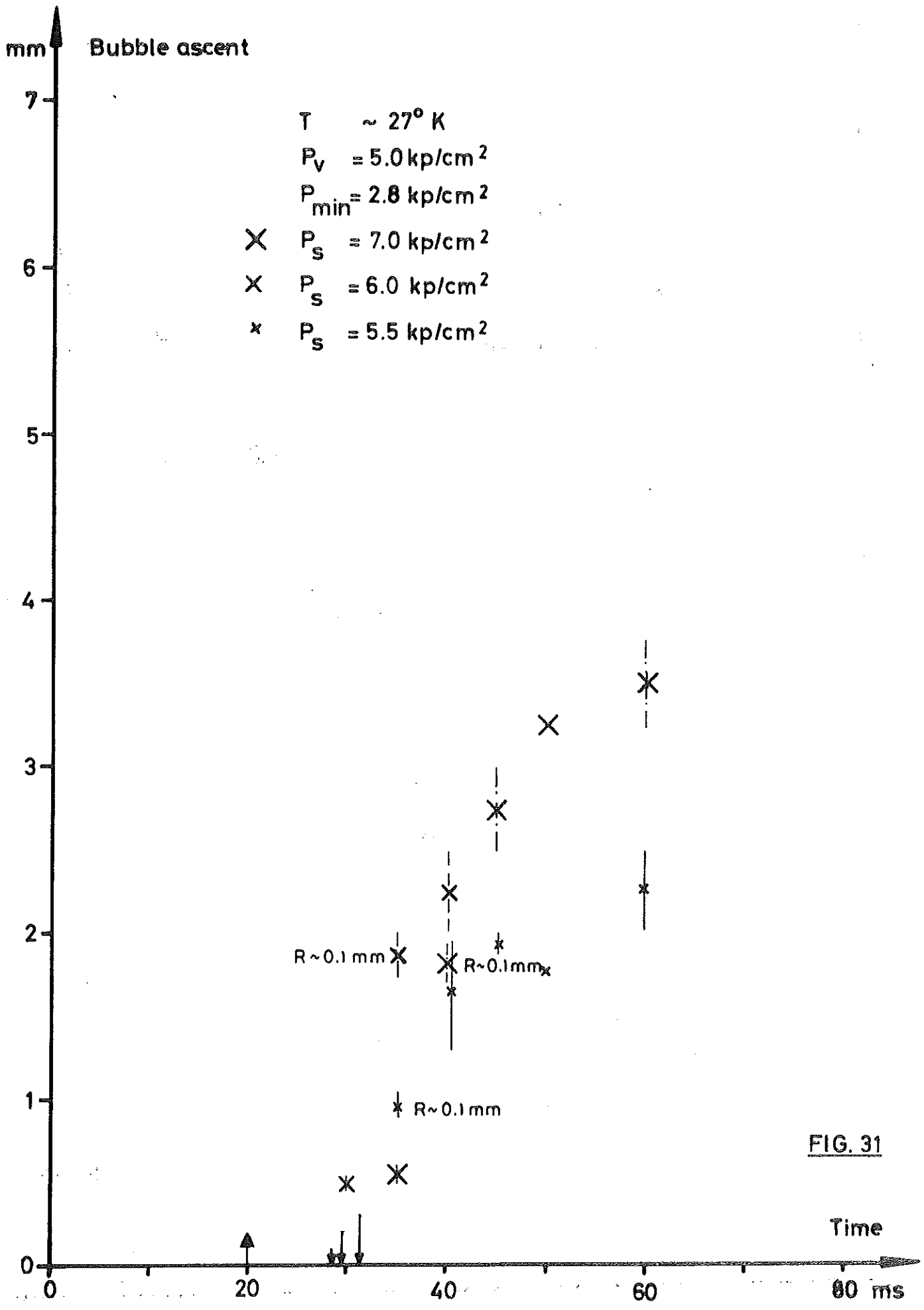
mm
Bubble ascent
7
6
5
4
3
2
1
0
T ~ 27° K
P_v = 5.0 kp/cm²
P_{min} = 2.8 kp/cm²
P_s = 7.0 kp/cm²
P_s = 6.0 kp/cm²
P_s = 5.5 kp/cm²
R ~ 0.1 mm
R ~ 0.1 mm
R ~ 0.1 mm
Time
0
20
40
60
80 ms

FIG. 31

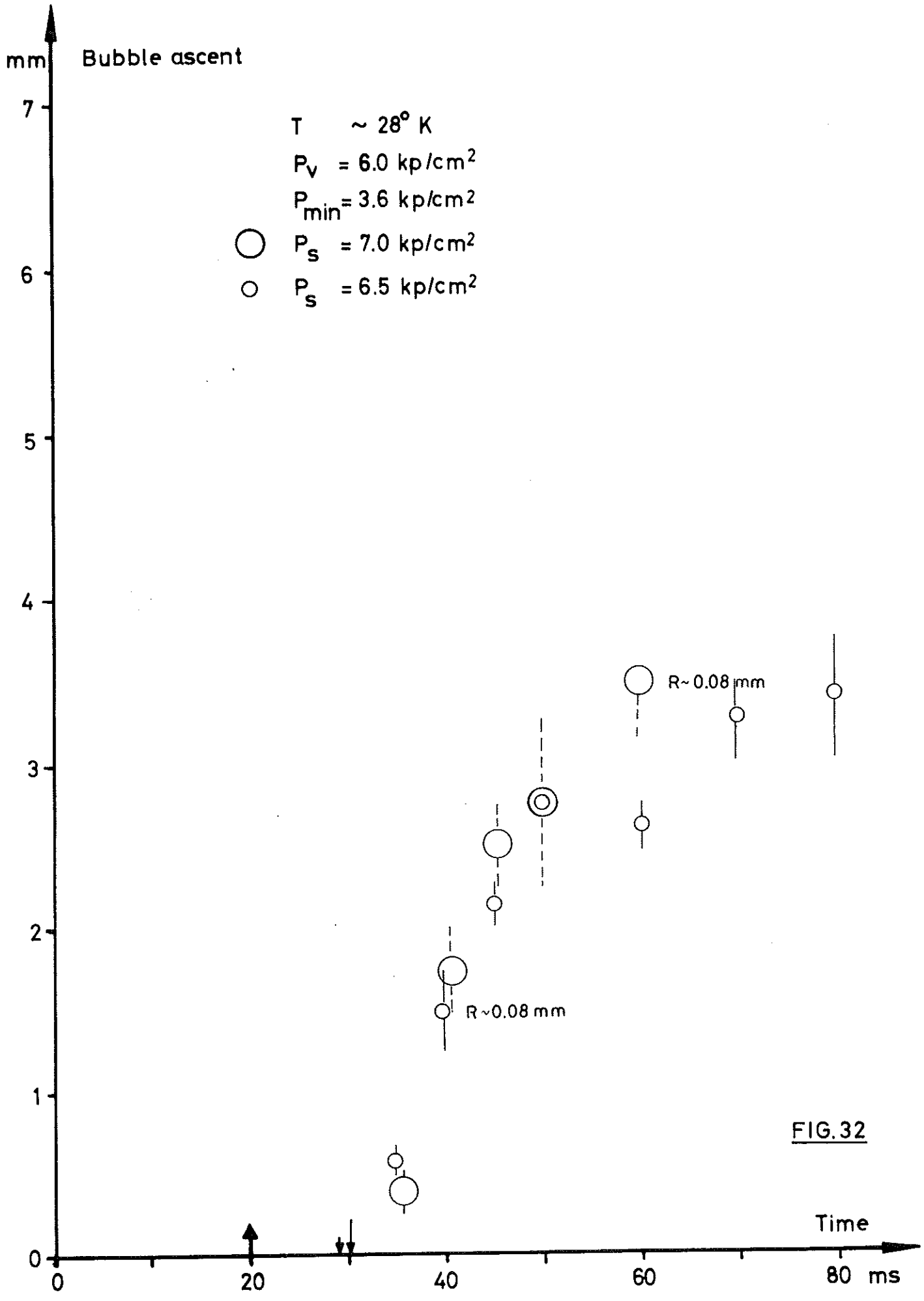
mm
Bubble ascent
T ~ 28° K
P_v = 6.0 kp/cm²
P_{min} = 3.6 kp/cm²
P_s = 7.0 kp/cm²
P_s = 6.5 kp/cm²
R~0.08 mm
R~0.08 mm
Time
0
20
40
60
80 ms
1
2
3
4
5
6
7

FIG. 32

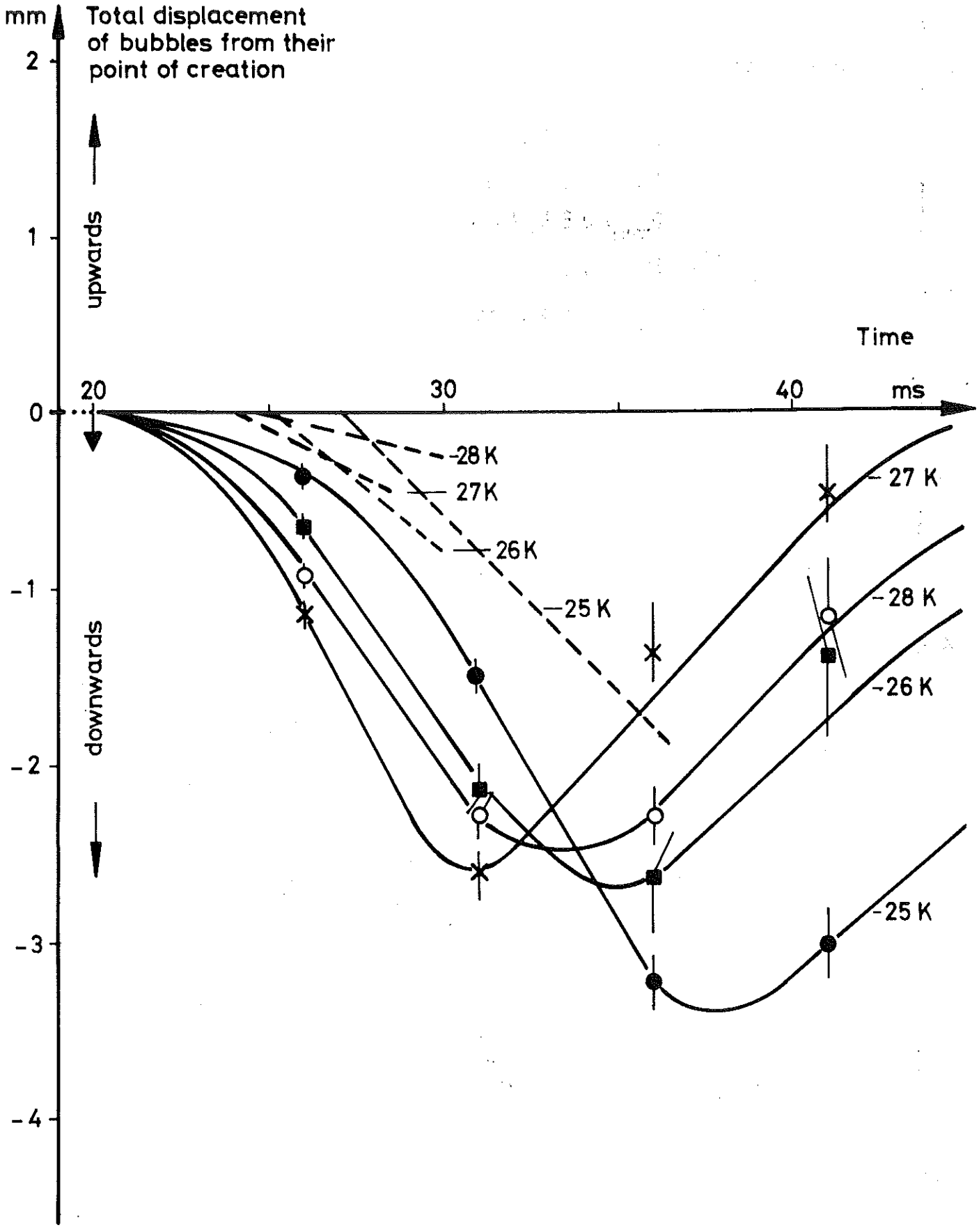
mm
Total displacement
of bubbles from their
point of creation
2
1
upwards
Time
20
30
40
ms
0
-28 K
-27K
-26K
-25 K
-1
downwards
-2
-3
-4
-27 K
-28 K
-26 K
-25 K

FIG. 33

Figs. 34a - 36a $T = 26$ K

$P_v = 4.15$ kp/cm^2

$P_s = 4.70$ kp/cm^2

$P_{min} = 1.80$ kp/cm^2

Fig. 34a $\Delta t = 1$ ms, $R \sim 0.11$ mm, $b \sim 23$ bubbles/cm

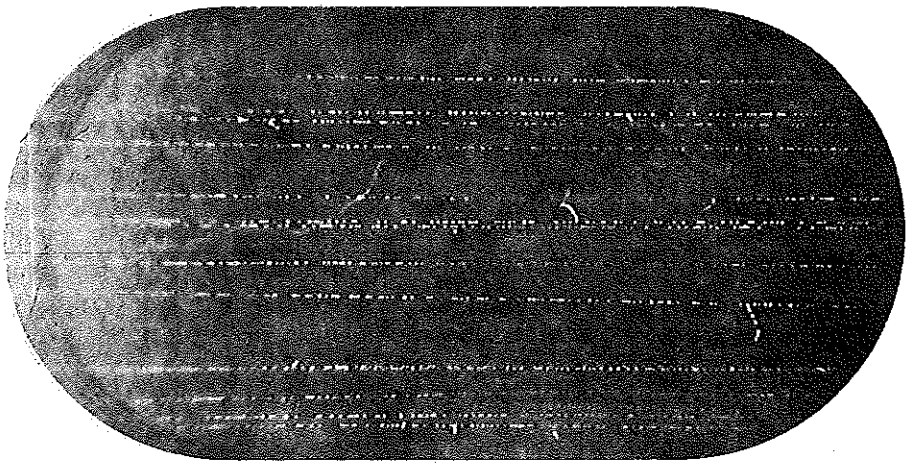

Fig. 35a $\Delta t = 3$ ms, $R \sim 0.20$ mm, $b \sim 20$ bubbles/cm

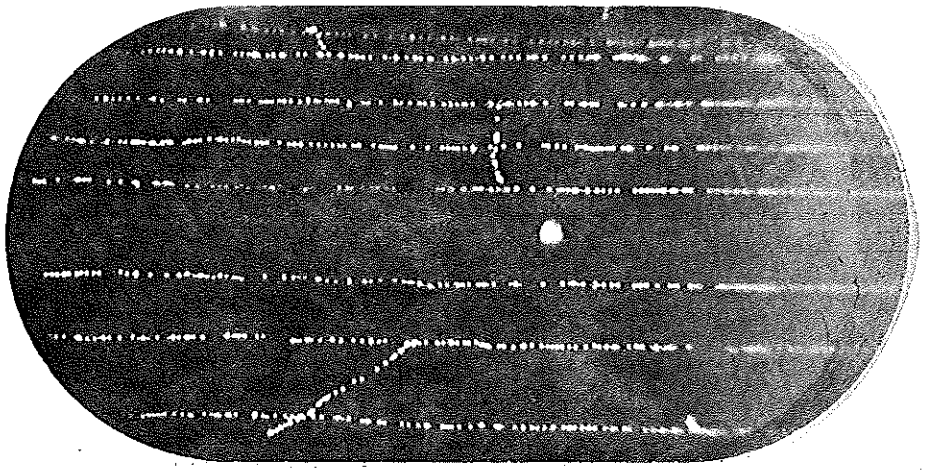

Fig. 36a $\Delta t = 5$ ms, $R \sim 0.25$ mm, $b \sim 15$ bubbles/cm

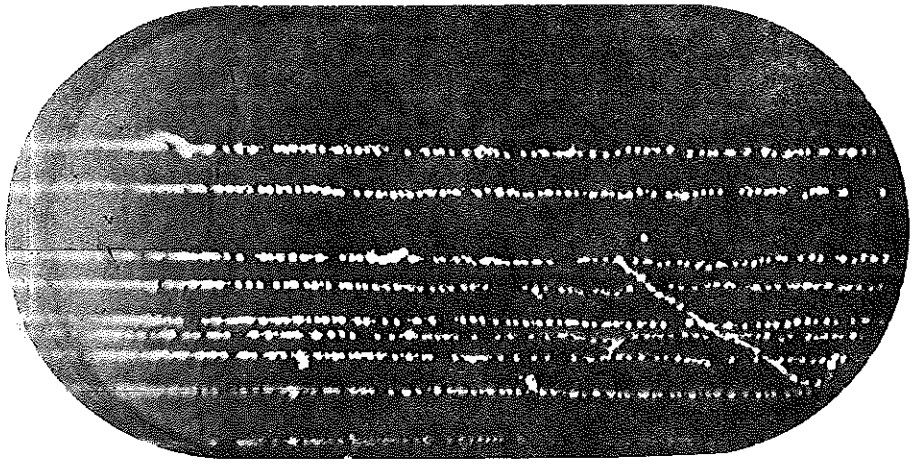

Figs. 37a - 39a $T = 27$ K

$P_v = 5.00$ kp/cm^2

$P_s = 5.49$ kp/cm^2

$P_{min} = 2.85$ kp/cm^2

Fig. 37a $\Delta t = 1$ ms, $R \sim 0.04$ mm, $b \sim 35$ bubbles/cm

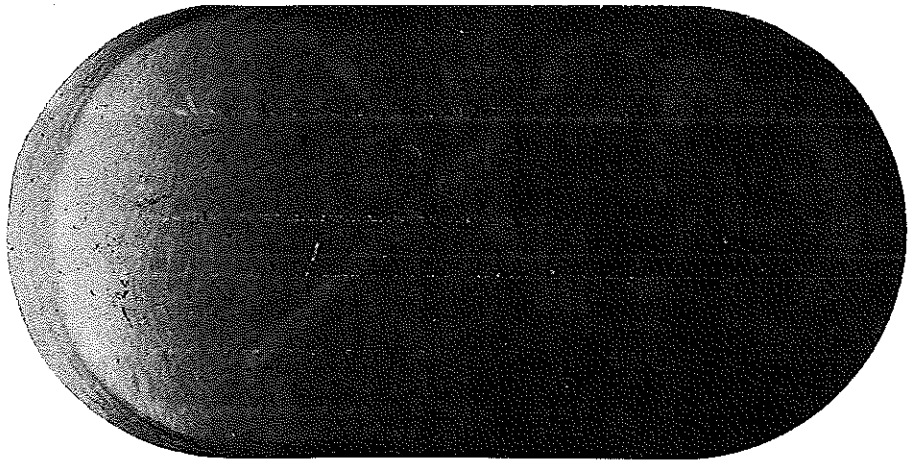

Fig. 38a $\Delta t = 3$ ms, $R \sim 0.07$ mm, $b \sim 25$ bubbles/cm

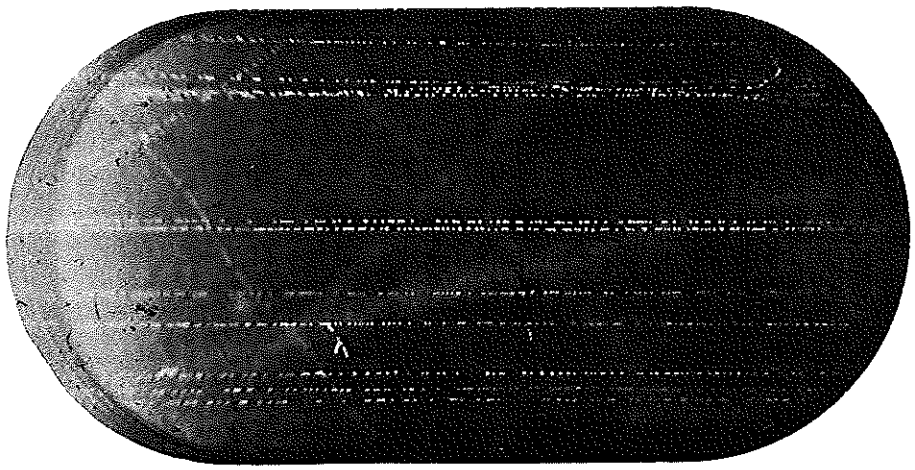

Fig. 39a $\Delta t = 5$ ms, $R \sim 0.12$ mm, $b \sim 22$ bubbles/cm

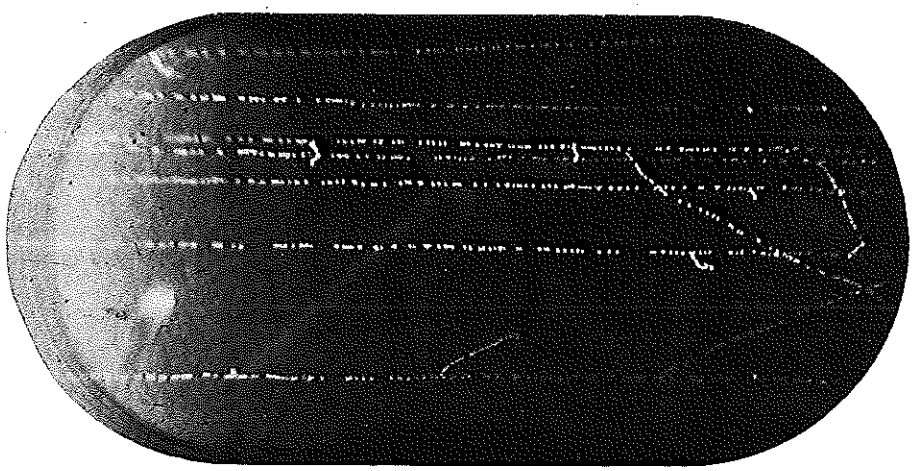

Figs. 40a - 42a

$T = 28$ K

$P_v = 6.00$ kp/cm^2

$P_s = 6.50$ kp/cm^2

$P_{min} = 3.70$ kp/cm^2

Fig. 40a $\Delta t = 1$ ms, R~0.05 mm, b~40 bubbles/cm

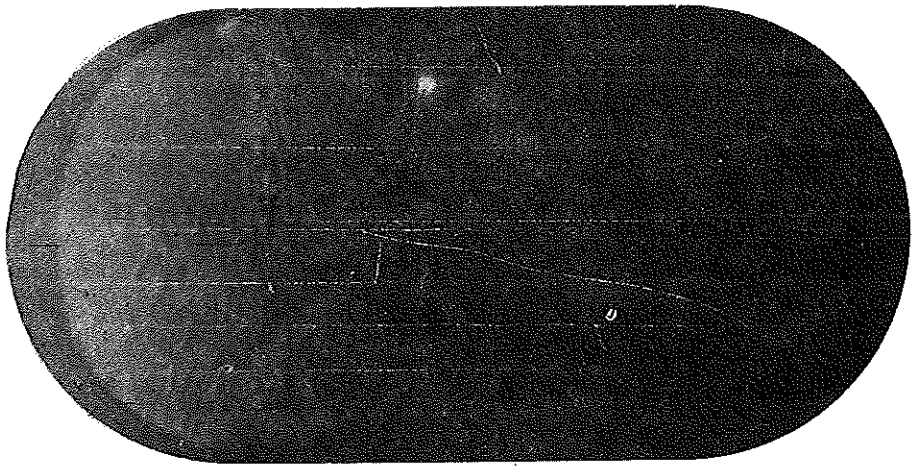

Fig. 41a $\Delta t = 3$ ms, R~0.09 mm, b~33 bubbles/cm

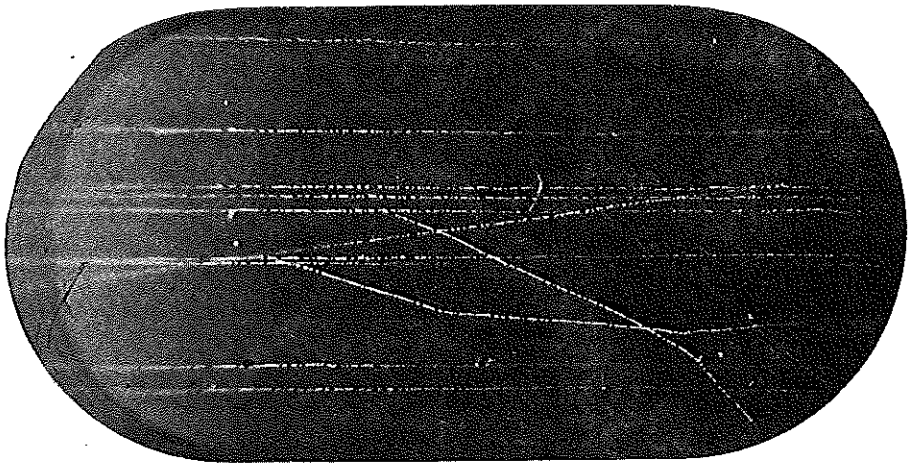

Fig. 42a $\Delta t = 5$ ms, R~0.11 mm, b~30 bubbles/cm

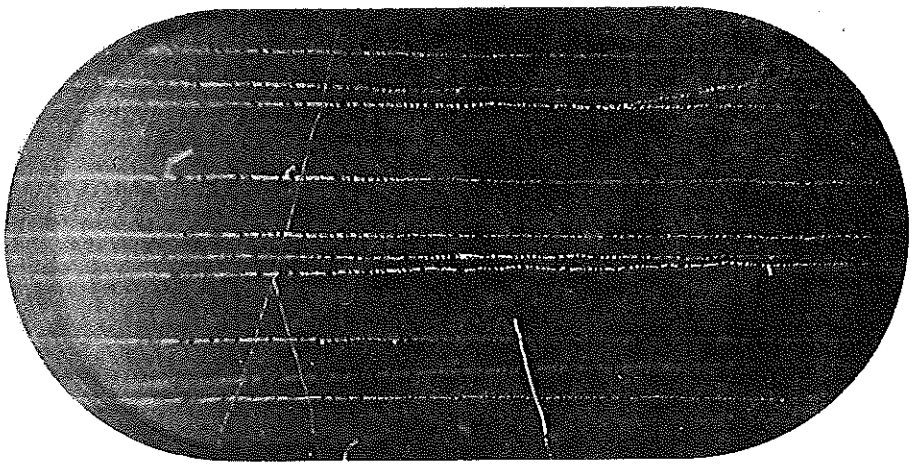

Figs. 34b - 36b $T = 26$ K

$P_v = 4.10$ kp/cm^2

$P_s = 6.10$ kp/cm^2

$P_{min} = 1.70$ kp/cm^2

Fig. 34b $\Delta t = 1$ ms, $R \sim 0.11$ mm, $b \sim 20$ bubbles/cm

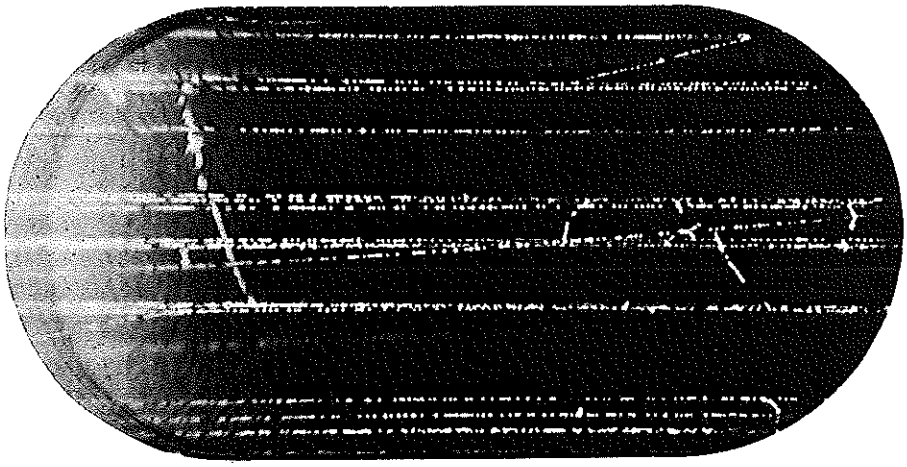

Fig. 35b $\Delta t = 3$ ms, $R \sim 0.21$ mm, $b \sim 18$ bubbles/cm

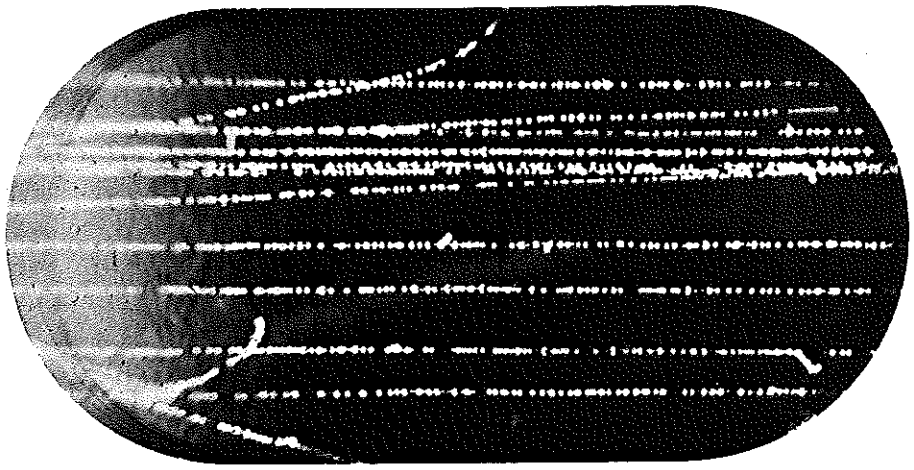

Fig. 36b $\Delta t = 5$ ms, $R \sim 0.30$ mm, $b \sim 14$ bubbles/cm

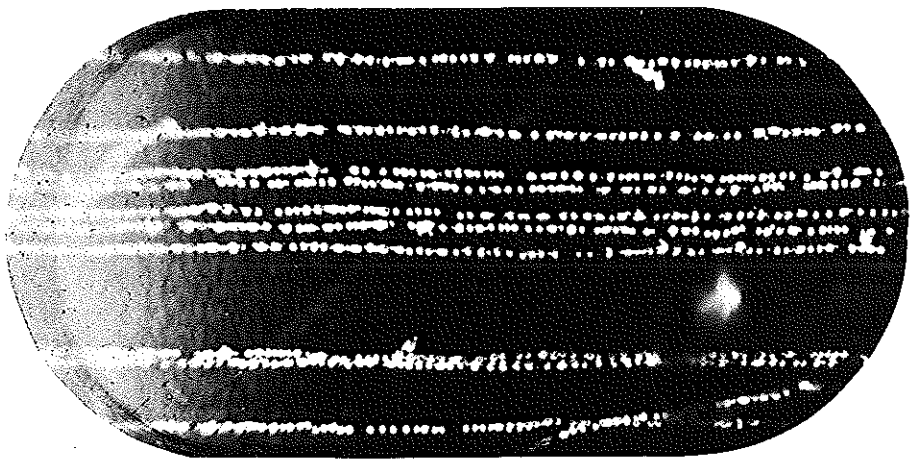

Figs. 37b - 39b $T = 27$ K

$P_v = 5.00$ kp/cm^2

$P_s = 6.98$ kp/cm^2

$P_{min} = 2.70$ kp/cm^2

Fig. 37b $\Delta t = 1$ ms, $R \sim 0.08$ mm, $b \sim 30$ bubbles/cm

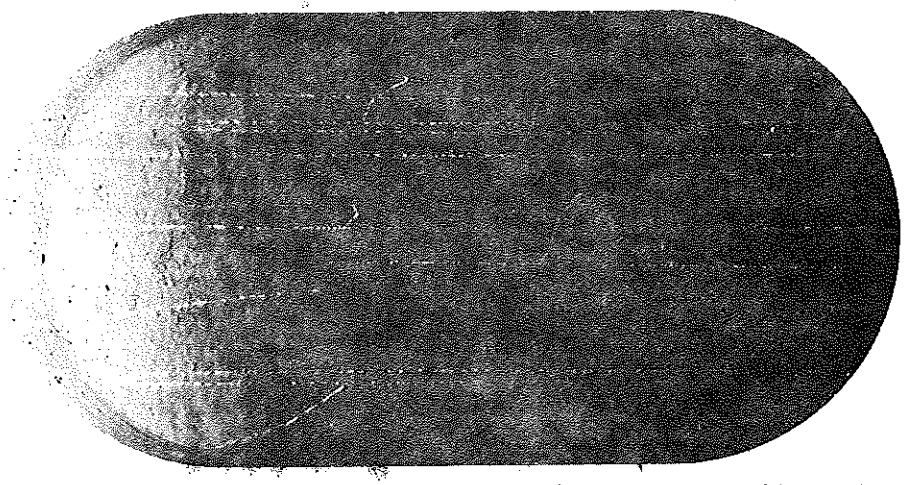

Fig. 38b $\Delta t = 3$ ms, $R \sim 0.16$ mm, $b \sim 21$ bubbles/cm

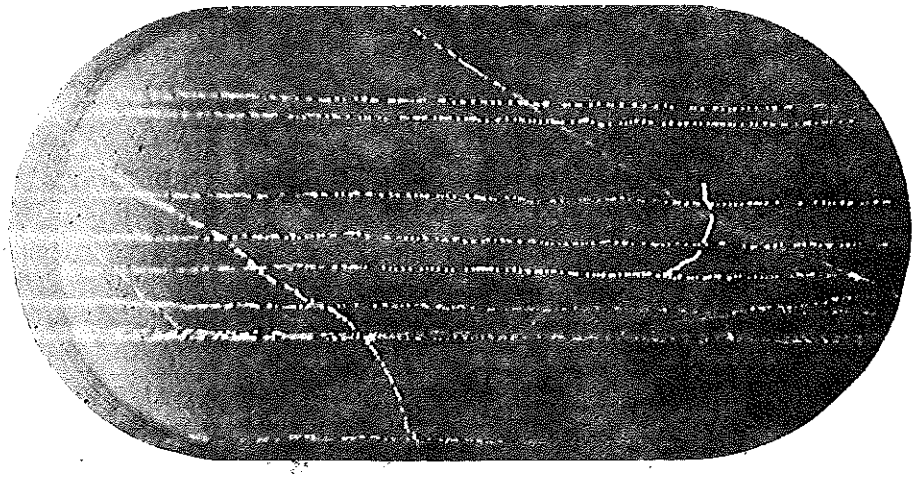

Fig. 39b $\Delta t = 5$ ms, $R \sim 0.16$ mm, $b \sim 18$ bubbles/cm

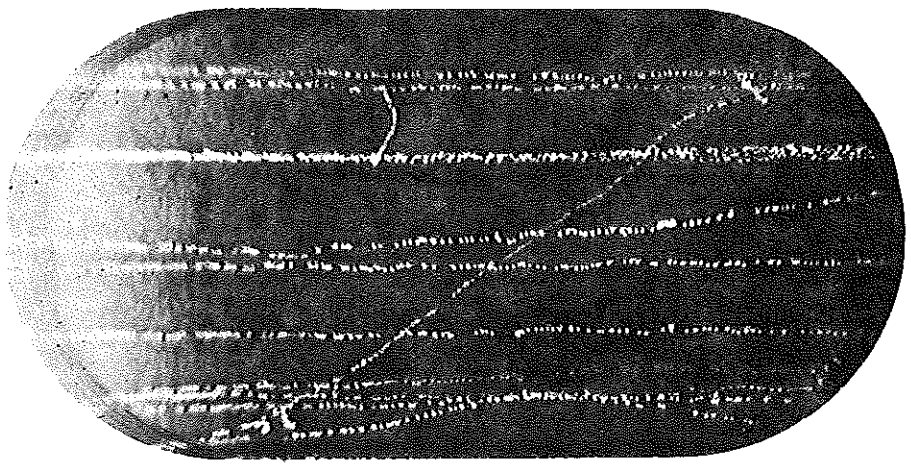

Figs. 40b - 42b

$T = 28$ K

$P_v = 6.00$ kp/cm^2

$P_s = 7.00$ kp/cm^2

$P_{min} = 3.60$ kp/cm^2

Fig. 40b $\Delta t = 1$ ms, $R \sim 0.05$ mm, $b \sim 48$ bubbles/cm

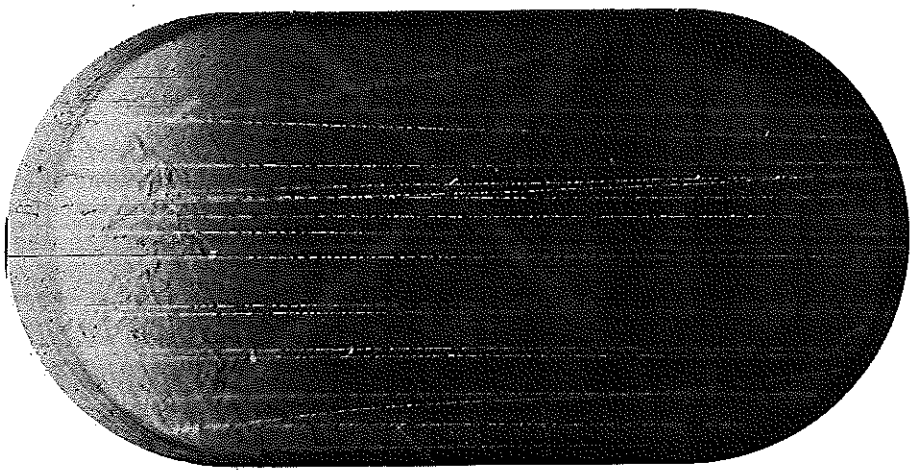

Fig. 41b $\Delta t = 3$ ms, $R \sim 0.08$ mm, $b \sim 45$ bubbles/cm

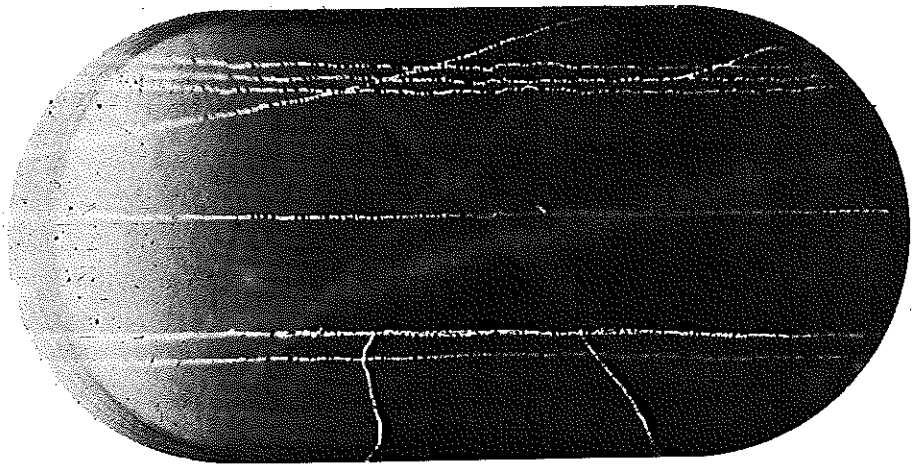

Fig. 42b $\Delta t = 5$ ms, $R \sim 0.14$ mm, $b \sim 35$ bubbles/cm